

## A MULTIWAVELENGTH STUDY OF STEPHAN'S QUINTET

JACK W. SULENTIC

Department of Physics and Astronomy, University of Alabama, Tuscaloosa, AL 35487

MARGARITA ROSADO AND DEBORAH DULTZIN-HACYAN

Instituto de Astronomía, Universidad Nacional Autónoma de México, Apdo. Postal 70-264, 04510 México D. F., Mexico

LOURDES VERDES-MONTENEGRO

Instituto de Astrofísica de Andalucía, Apdo. Postal 3004, E-18080 Granada, Spain

GINEVRA TRINCHIERI

Osservatorio Astronomico di Brera, via Brera 28, I-20121 Milano, Italy

CONG XU

IPAC, California Institute of Technology, 7700 South Wilson Avenue, Pasadena, CA 91125

AND

WOLFGANG PIETSCH

Max-Planck-Institut für Extraterrestrische Physik, Postfach 1312, D-85741 Garching, Germany

Received 2001 July 2; accepted 2001 September 20

### ABSTRACT

Stephan's Quintet (SQ) is a compact group that we find in an atypical moment when a high-velocity intruder is passing through it. The intrusion is particularly interesting because a previous intruder had stripped most of the gas from the group members. This debris field was shocked in the ongoing collision with the new intruder. This evolutionary history agrees well with observations and explains how a strongly interacting system can show low levels of star formation. We present new multiwavelength data including previously unpublished *ROSAT* X-ray, H $\alpha$  interference filter/Fabry-Pérot, *ISO* MIR/FIR, and radio line and continuum images. These observations and previously published data provide new insights, as well as support for some previous hypotheses. (1) Fabry-Pérot and H I velocities allow us to unambiguously distinguish between gas associated with SQ and the new intruder. (2) Most detected emission regions are found in the remnant interstellar medium (ISM) of the new intruder, which allows us to infer its size and present physical state. (3) The few emission regions associated with the stripped ISM of SQ include the best candidate tidal dwarf galaxy. (4) Multiwavelength data suggest that strong MIR/FIR emission from the Seyfert 2 nucleus of NGC 7319 comes from dust heated directly by a power-law continuum rather than a starburst. (5) The correspondence between extended X-ray/radio continuum/forbidden optical emission confirms the existence of a large scale shock in SQ. (6) We confirm the presence of two stripped spiral members in the process of transformation into E/S0 morphology. Finally (7) observations are consistent with the idea that the collision in SQ is ongoing with possible detection of H II region ablation and Rayleigh-Taylor instabilities.

*Key words:* galaxies: interactions — galaxies: kinematics and dynamics — galaxies: structure — galaxies: Seyfert — intergalactic medium

### 1. INTRODUCTION

Compact groups are aggregates of four or more galaxies showing projected separations on the order of  $\sim 30$ – $40$  kpc (assuming  $H_0 = 75 \text{ km s}^{-1} \text{ Mpc}^{-1}$ ), which imply space densities similar to the cores of rich clusters. Compact groups are high-density fluctuations usually located in noncluster environments (Sulentic 1987; Rood & Williams 1989). Their importance is twofold: (1) they are ideal laboratories for studying the effects of extreme galaxy interactions, and (2) they are low-redshift analogs of processes believed to be very important at high redshift. One can study the groups either statistically or individually. The former approach still suffers from effects of sample selection bias and incompleteness. For example, only 60 of the 100 groups cataloged by Hickson (1982) actually satisfy the initial selection criteria (Sulentic 1997). The remaining objects either violate the selection criteria, extend them beyond the originally stated limits, or involve triplets (with a fourth discordant-redshift galaxy projected). Since it is unclear whether triplets share the same properties as  $N > 3$  accordant redshift systems, it appears safer at present to treat them separately. In

any case, if they represent groups in the process of formation by sequential acquisition of neighbors, they will not show the same level of interaction induced phenomena as richer systems. We note that 16 triplets included in the compact group sample studied by Verdes-Montenegro et al. (2001) did not show the significant hydrogen deficiency found for systems with four or more members. Triplets also show larger velocity dispersions than  $n \geq 4$  systems (Sulentic 2000) suggesting that they may be unbound systems. A new southern hemisphere sample of compact groups (Prandoni, Iovino, & MacGillivray 1994; Iovino 2000), selected with automated techniques, promises to minimize and quantify effect of bias when a suitable multi-wavelength database better defines its properties.

Stephan's Quintet (SQ) is the ideal candidate for detailed study because it is bright and because it is in a rare but important stage of dynamical evolution. Inferring group properties from SQ is not unreasonable because it is typical of the compact group phenomenon as defined in the Hickson (1982) catalog (see also Prandoni et al. 1994), only showing more spectacular properties because of an ongoing

collision. The best example of an “active” compact group in the southern hemisphere may involve the Cartwheel galaxy (Wolter, Trinchieri, & Iovino 1999), where the most recent collision occurred a few times  $10^8$  yr ago. The crossing time for such collisions is so short (a few times  $10^7$  yr) that more than one “SQ” is unlikely to be found in a sample of 100 compact groups. The frequency of such collisions is a direct function of local galaxy density, and SQ is not in an unusually dense environment (Sulentic 1987). The distribution of component velocities relative to the first-ranked member in Hickson groups (Sulentic 2000) suggests that SQ is not the only group with a possible high-velocity intruder nearby.

A “two-intruder” (old intruder = NGC 7320c = OI; new intruder = NGC 7318b = NI) evolutionary model has been proposed for SQ (Moles, Sulentic, & Marquez 1997) that may be relevant to most compact groups and that may

have relevance for our understanding of interactions at high redshift. This model forms the basis for our interpretations of the multiwavelength data. In § 2 we discuss the new observations and their reductions, as well as data harvested from archival sources. In § 3 we discuss past work on SQ and compact groups in general. We combine new and old observations in § 4 to show how they are consistent with the two-intruder scenario. Section 5 summarizes important results and their implications.

## 2. NEW AND HARVESTED MULTIWAVELENGTH OBSERVATIONS

We present new observations at X-ray, optical, infrared, and radio wavelengths, as well as optical archival data that include the highest-resolution (*HST*) and highest-sensitivity (California-France-Hawaii Telescope [CFHT]) optical images. Figure 1 gives finding charts for SQ.

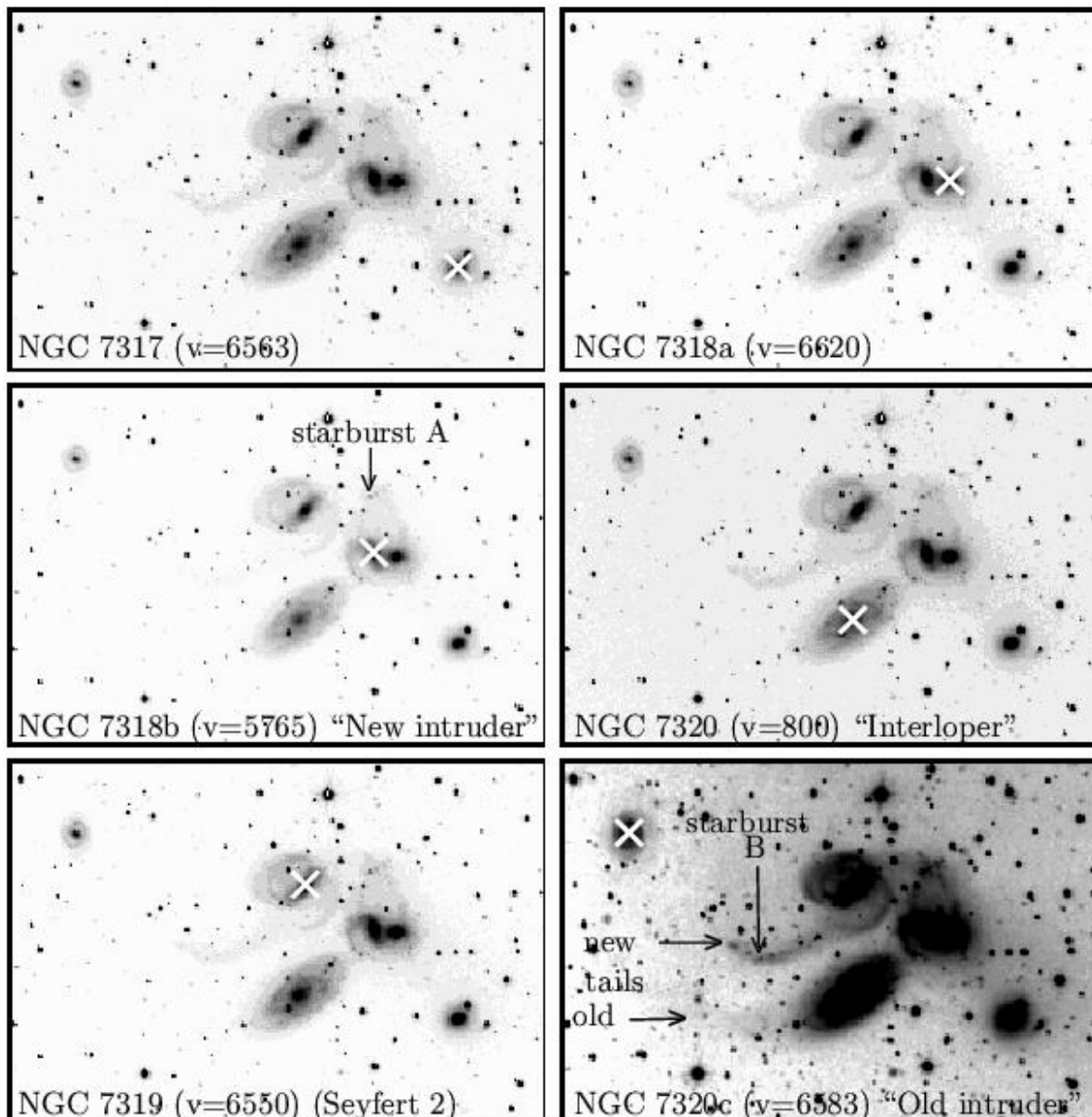


FIG. 1.—Finding charts for each galaxy in SQ where the recession velocities and aliases are also noted. Other important features discussed in the text are identified. The new and old tail in the lower right panel are, respectively, synonymous with the younger and older tail in the text.

### 2.1. *ROSAT* X-Ray

We obtained new *ROSAT* HRI (Trümper 1983; Pfeffermann et al. 1987) data in 1996 December to 1997 January with a total observing time of 65 ks split into 35 intervals (OBIs). These observations followed a shorter one ( $\sim 23$  ks), already discussed (Pietsch et al. 1997), which we also include in the present analysis. We excised time patches of data shorter than 40 s (caused by high background rejection in the standard analysis and/or high-voltage excursions, for a total of 600 s) and lowered the tolerance to low count rates that excludes a higher percentage of high-particle background data, mostly in proximity to radiation belts. This screening resulted in a loss of 6.4 ks of data, but it should ensure a very clean data set. The same cleaning was applied to the old data set, so the total observing time on SQ is  $\sim 77.5$  ks.

Due to the lack of strong point sources in the HRI field of view, we could not improve on the short-term aspect solution used by the Standard Analysis Software System (SASS, Voges et al. 1992). However, we verified that no major time-dependent effects are present in the data by accumulating and comparing images in three  $\sim 20$  ks intervals. We found that (1) the positions of the few field sources were the same, and (2) a possible residual systematic effect of improper wobbling might still be present. Further checks confirmed a residual wobbling-related effect, so that no structure on scales of  $7''$ – $10''$  could be trusted. We also evaluated the absolute pointing of the observations by searching for optical counterparts to all of the X-ray detections in the field of SQ. None of the sources outside of SQ coincide with known objects (e.g., from SIMBAD or NED), but faint counterparts are visible on the DSS2 for three sources. We realigned the absolute coordinates of the X-ray map on these sources, using in addition the radio position of the Seyfert nucleus (van der Hulst & Rots 1981). This produced a  $0.4$  shift to the east. Our final positions should be accurate to  $2''$ – $3''$ .

We considered merging both HRI data sets in order to improve the statistical significance of our results. However, since the source is not at the same detector position in both pointings (it was  $\sim 4'$  off axis in the first observation) and in light of known spatial inhomogeneities in detector gain, which also changes with time,<sup>1</sup> we decided against it, and we use the data sets independently. Most of the following discussion is based on the second and longer observation, with the shorter one used for consistency checks. To limit the changes due to gain effects, while improving on the signal-to-noise ratio, we have selected data in PHA channels 1 to 10 for both observations, which considerably reduces the background contribution (see also the on-line documentation; note that this is a larger range than used in Pietsch et al. 1997, where only PHA channels 4–8 were included). The background was obtained from a  $4'$ – $6'$  annulus around the field center in both data sets. In the first observation, since the source itself is at  $\sim 4'$  off axis and is therefore included in this annulus, a circle of  $3'$  radius centered on SQ is masked out from the background region.

Figure 2 (*left*) shows two X-ray images of SQ involving: (1) adaptively smoothed (*top*) and (2) Gaussian filtered (*bottom*) data. The adaptive smoothing algorithm provided

with the CIAO software was used.<sup>2</sup> We have used the FFT method with  $2\sigma$  minimum significance. Table 1 summarizes the contribution of each feature to the old and the new observations. The flux is obtained from the total count rate, converted assuming a *Raymond* spectrum with  $kT = 1$  keV and the line-of-sight Galactic absorption  $N_{\text{H}} = 7 \times 10^{20}$   $\text{cm}^{-2}$ . The flux determination is almost independent of the choice of a spectral model, given the relatively narrow energy range of *ROSAT*, for reasonable values of the absorbing column density (see Pietsch, Trinchieri, & Vogler 1998). This assumption will not be correct if significant absorption is present, e.g., in the Seyfert 2 nucleus. We have defined four regions: (1) a circle at the position of the Seyfert galaxy NGC 7319, with  $r = 18''$ ; (2) a circle at the position of NGC 7318a ( $r = 15''$ ); (3) a rectangle of  $0.9 \times 1.6$ , centered on the elongated north-south feature; and (4) a smaller rectangle ( $0.4 \times 0.8$ ) that includes only the higher surface brightness part of this feature.

Figure 2 shows (*b*) 21 cm radio continuum and (*d*) forbidden  $[\text{N II}] \lambda 6583$  images. The radio image (see § 2.5) shows the same structure as the X-ray in (1) the elongated feature (interpreted as a collisional shock), (2) the extension of this feature to the extreme northwest of SQ, and (3) the detection of the elliptical galaxy member NGC 7318a. The radio continuum image of the extended feature is relatively stronger and broader on the south edge, which may reflect attenuation of the X-ray emission due to the larger hydrogen column of foreground NGC 7320 that extends over this region. The peak H I column in NGC 7320  $N_{\text{H}} = 1.6 \times 10^{21}$   $\text{cm}^{-2}$  is slightly more than twice Galactic, and the distribution of H I is flat so that there is more than double Galactic column ( $9.0 \times 10^{20}$   $\text{cm}^{-2}$  from NGC 7320 and  $7.0 \times 10^{20}$   $\text{cm}^{-2}$  from the Milky Way) in the region where the X-ray emission from the shock is weakest relative to radio continuum.

We attempted to quantify the significance of any low surface brightness component that might be present in SQ by measuring emission in several features visible on the X-ray maps. Figure 3 shows the azimuthally averaged profile of the total emission as well as the emission averaged in two opposite quadrants along the north-south and east-west directions. We derived the profiles in concentric annuli of increasing size, centered on the peak of the emission in the extended feature as seen in the adaptively smoothed map (Fig. 2*a*). The azimuthally averaged profile shows a clear excess over the background out to  $r \sim 1.5$ . The emission appears to be extended roughly equally in the north-south and in the east-west directions. Some very low surface brightness emission could extend to  $r \sim 3'$ , mostly in the east-west direction (Fig. 3*b*). Recently obtained *Chandra* data confirm the existence of such emission (Trinchieri et al. 2001).

### 2.2. *H $\alpha$* Interference Filter Imaging

Interference filter observations were obtained in 1997 August with the 2.2 m telescope at Observatorio Astronómico Hispano Aleman on Calar Alto, Spain (see also Xu, Sulentic, & Tuffs 1999). They are not the first emission-line images obtained for SQ (Arp 1973; Moles et al. 1997; Vilchez & Iglesias-Paramo 1998b; Severgnini et al. 1999), but they are the most sensitive, cover the entire group, and

<sup>1</sup> See the discussion in the *ROSAT* HRI Calibration Report and Users' Handbook, available on-line at <http://hea-www.harvard.edu/rosat>.

<sup>2</sup> See <http://asc.harvard.edu> for further details.

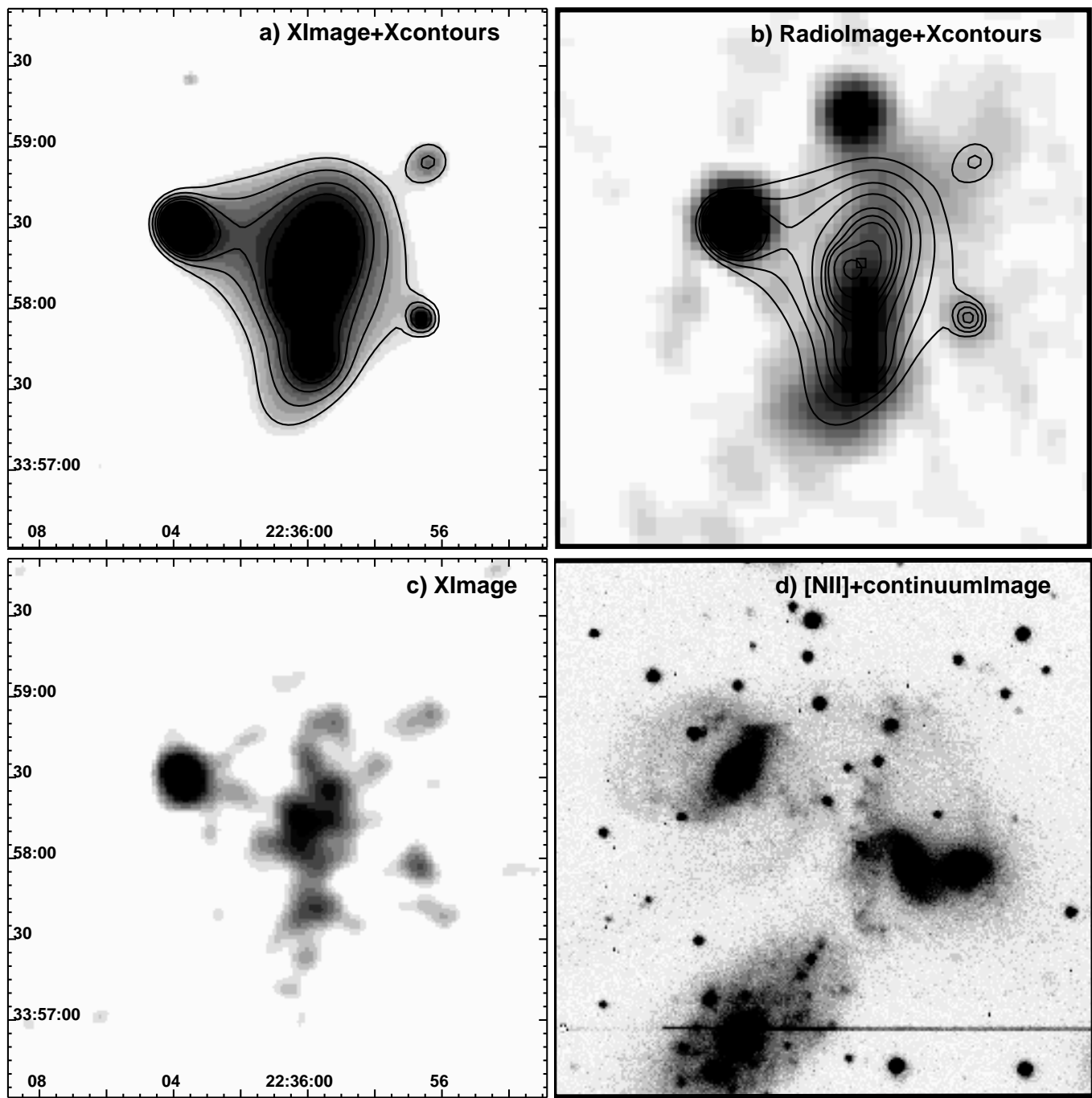


FIG. 2.—Comparison of the X-ray maps from the new HRI observation of Stephan's Quintet with radio continuum and  $[\text{N II}]$  line + red continuum emission. (a) Adaptively smoothed HRI image with superposed contours. (b) Adaptively smoothed HRI contours superposed on a 21 cm radio continuum image ( $18''$  synthesized beam) with comparable effective resolution. (c) Gaussian-smoothed ( $\sigma = 4''$ ) HRI image. (d) Interference filter image centered at  $6731 \text{ \AA}$  (FWHM =  $10 \text{ \AA}$ ) sensitive to  $[\text{N II}] \lambda 6583$  (+ continuum) emission in the SQ velocity range  $6460\text{--}7000 \text{ km s}^{-1}$ .

effectively separate group from NI emission. Two narrow-band filters (667/7 and 674/8) centered at  $6667 \text{ \AA}$  (FWHM =  $66 \text{ \AA}$ ) and  $6737 \text{ \AA}$  (FWHM =  $76 \text{ \AA}$ ) allowed us to separate most of the SQ emission ( $6300\text{--}7000 \text{ km s}^{-1}$ ) from that of the NI ( $5600\text{--}6000 \text{ km s}^{-1}$ ). The  $\text{H}\alpha$  transmission for the 667/7 filter was 0.49 for the  $5700 \text{ km s}^{-1}$  emission and 0.04 for SQ emission, while the 674/8 filter yielded a transmission of 0.49 for SQ and 0.06 for  $5700 \text{ km s}^{-1}$  emission. The region of strongest overlap involves emission from the NI at  $\sim 6000 \text{ km s}^{-1}$  located north of the nucleus. The continuum was subtracted from both images using an

$R$ -band image. Both maps were smoothed with a  $2''$  Gaussian beam in order to increase sensitivity to diffuse emission (Xu, Sulentic, & Tuffs 1999). Figure 4 shows the emission line images for SQ (*top*) and NI (*bottom*), while Figure 5 shows the same images with relevant  $\text{H I}$  contours overlaid on them. Contours represent  $\text{H I}$  velocity ranges (*top*)  $6500\text{--}6800 \text{ km s}^{-1}$  and (*bottom*)  $5600\text{--}6000 \text{ km s}^{-1}$ . Figure 6 (*bottom*) shows the appropriate wavelength ranges where emission from  $\text{H}\alpha$ ,  $[\text{N II}] \lambda 6583$  and the  $[\text{S II}]$  doublet  $\lambda\lambda 6717, 6731$  are observed. In the bottom panel we also indicate the filters used with appropriate FWHM. The

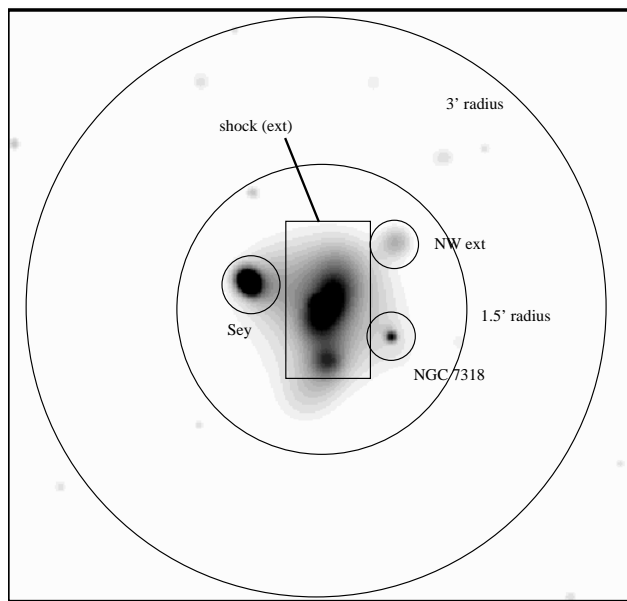


FIG. 3a

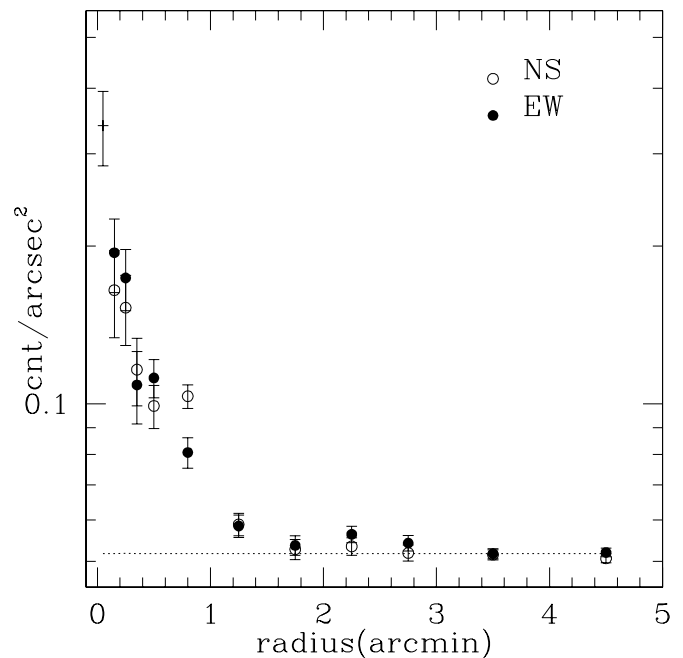


FIG. 3b

FIG. 3.—(a) Schematic of the regions for which X-ray fluxes were derived and tabulated in Table 1. (b) Radial distribution of the total emission from SQ, azimuthally averaged in two arcs oriented north-south, in concentric annuli about the X-ray peak roughly in the middle of the elongated north-south extended source. The adopted background level is also shown. The excess at  $r \sim 1'$  is due to the Seyfert nucleus. Data are from the new observation only.

diagram allows one to assess the degree of overlap for all the interference filter observations described in this paper.

We also used the 2.1 m telescope at Observatorio Astronómico Nacional (at San Pedro Mártir, Baja California, México) to obtain three 20 minute exposures through a narrowband filter centered at  $6731 \text{ \AA}$  (FWHM =  $10 \text{ \AA}$ ). The observations were made with the Fabry-Pérot interferometer instrument (PUMA without an etalon) in the direct imaging mode. The resultant images are sensitive only to  $[\text{N II}] \lambda 6583$  (+continuum) emission in the  $6740\text{--}6970 \text{ km s}^{-1}$  velocity range (SQ ISM) and should therefore image diffuse  $[\text{N II}]$  emission associated with the shock, as well as discrete emission from H II regions. The full velocity range of this emission is estimated to be  $6300\text{--}7000 \text{ km s}^{-1}$  based upon our Fabry-Pérot measures. This image is shown in Figure 2d. Figure 6 indicates that we simultaneously image the  $[\text{S II}] \lambda 6717$  emission in NGC 7320, where several of the highest density H II regions are detected.

### 2.3. Fabry-Pérot $\text{H}\alpha$ Imaging

The observations were carried out during the nights of 1997 October 27, 28, and 30 and 1999 September 10 with the Fabry-Pérot (F-P) interferometer PUMA (Rosado et al. 1995) attached to the f/7.9 Ritchey-Chretien focus of the 2.1 m telescope at the Observatorio Astronómico Nacional. The PUMA setup is composed of a scanning F-P interferometer, a focal reducer with an f/3.95 camera, a filter wheel, a calibration system and a Tektronix  $1\text{K} \times 1\text{K}$  CCD detector. The main characteristics of the instrumental setup are the following: CCD readout was binned  $2 \times 2$ , giving a pixel size of  $1''.2$  (equivalent to  $\sim 500 \text{ pc}$  at  $90 \text{ Mpc}$ ) with a  $10' \times 10'$  field of view.

The F-P interferometer has an interference order of 330 at  $6563 \text{ \AA}$ , and its free spectral range of  $934 \text{ km s}^{-1}$  was

scanned in 48 steps with a sampling resolution of  $19 \text{ km s}^{-1}$ , yielding a data cube of  $48 \times 512 \times 512$  elements. F-P observations of SQ are complicated because of the wide range of velocities present in three overlapping ranges (see Fig. 6) and because the emission is so complex and extended. The large field of view and free spectral range of PUMA were indispensable for interpreting the F-P data. We obtained data cubes in the lines of  $\text{H}\alpha$  in the velocity range of the  $\text{NI}$  and  $[\text{N II}] (\lambda 6583)$  in the velocity range of SQ. No filter was available for a zero-order observation of  $\text{H}\alpha$ , but it appears at second order in our velocity cubes with almost identical channel-velocity correspondence (the velocity separation of the two lines is almost identical to the free spectral range of PUMA). During our first observing run we obtained two data cubes at  $6750 \text{ \AA}$ , three at  $6720 \text{ \AA}$ , and two at  $6680 \text{ \AA}$ , each one with an exposure time of  $60 \text{ s}$  per channel. During the second run we obtained three data cubes at  $6680 \text{ \AA}$ , each with  $120 \text{ s}$  integration time per channel. Similar quality data cubes were co-added in order to enhance the signal-to-noise ratio (S/N). We thus obtained total exposure times of 1.6, 2.4, and 1.6 hr for the observations at  $6750$ ,  $6720$ , and  $6680 \text{ \AA}$ , in the first observing run, respectively, and a total exposure time of 4.8 hr for the observations at  $6680 \text{ \AA}$  in the second observing run. The  $\pm 1$  orders fall at the edges (half-power points) of the filter ranges shown in Figure 6.

The phase calibration was made by taking data cubes of a calibration lamp before and after the SQ exposures. When the exposure times of the object data cubes were of more than 2 hours, we obtained an additional calibration data cube between object exposures in order to ensure that no instrument flexure had occurred. We used a neon line at  $6717.04 \text{ \AA}$  for calibrating the object cubes. Reductions were carried out using the software package CIGALE (Le Coarer et al. 1993). Our data cubes in  $\text{H}\alpha$  are contaminated with

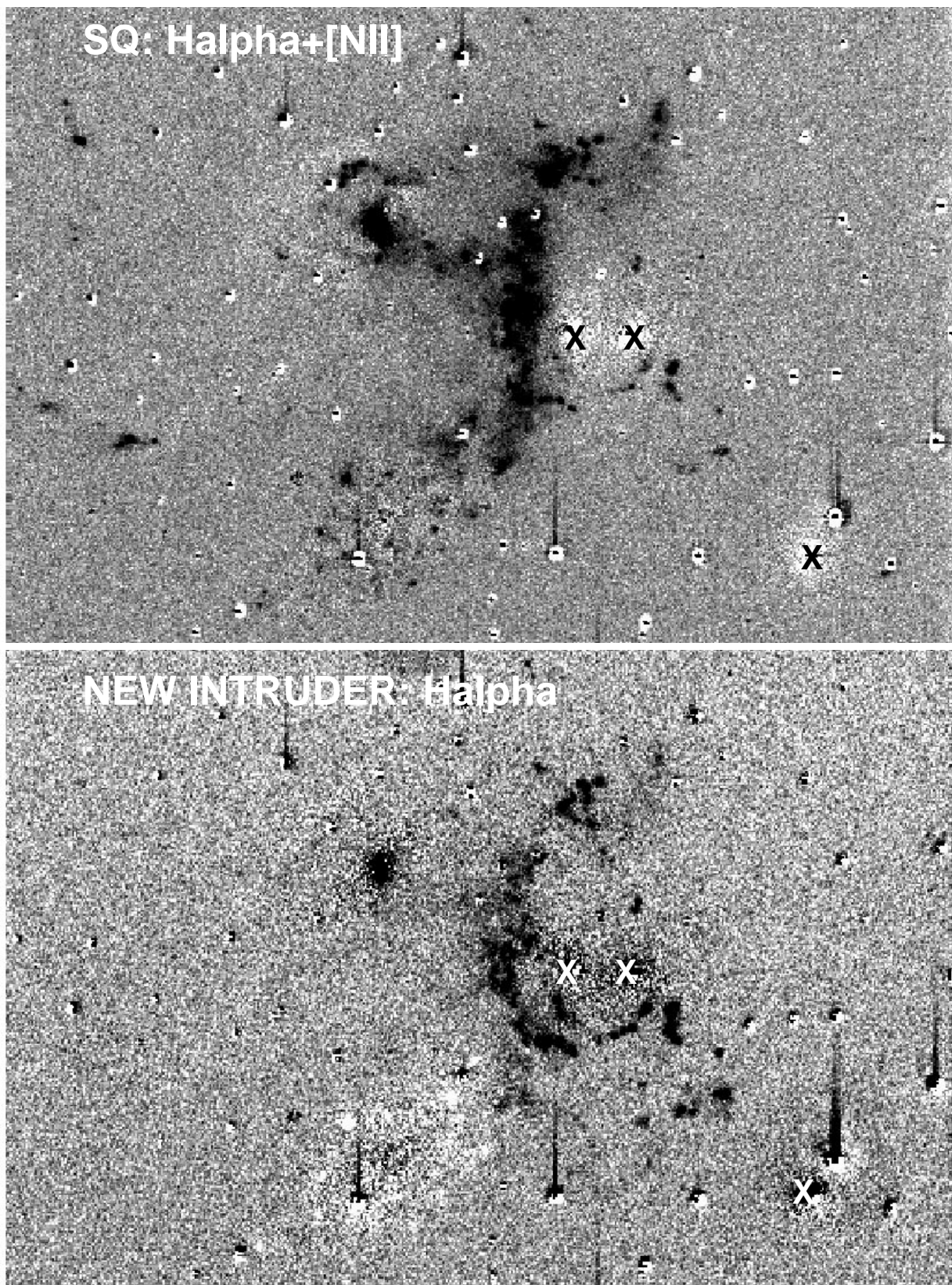


FIG. 4.—Interference filter images. *Top*: Continuum-subtracted line image centered at  $6738 \text{ \AA}$ , which includes  $H\alpha$  and  $[\text{N II}]$  emission from SQ. There is contamination from  $[\text{N II}]$  in the new intruder. *Bottom*: Equivalent image centered at  $6668 \text{ \AA}$  and imaging  $H\alpha$  emission in the new intruder. Contour maps for both images with appropriate flux levels can be found in Xu et al. (1999). The nuclei of NGC 7317, as well as NGC 7318a and NGC 7318b, are marked with an “X.” Scale can be obtained from the  $21''$  separation of the Xs for NGC 7318a and NGC 7318b.

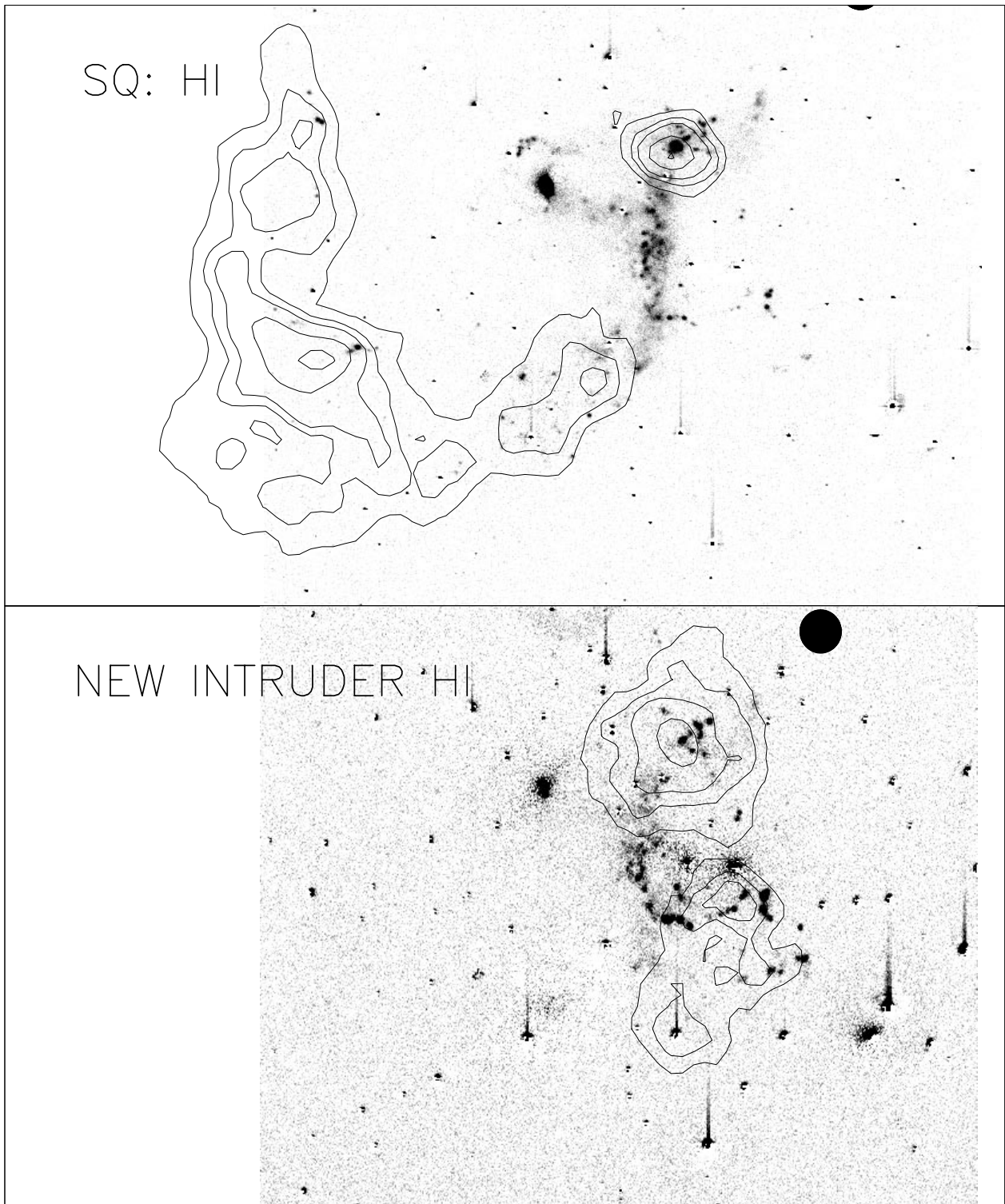


FIG. 5.—H I 21 cm radio contours superposed on the interference filter images. *Top*: H I contours for velocities in the SQ range 6475–6755 km s<sup>-1</sup>. *Bottom*: H I contours for velocities in the new intruder range (5597–6068 km s<sup>-1</sup>). H I contours levels correspond to 5.26e19, 1.58, 2.63, 5.26, 7.89 × 10<sup>20</sup> cm<sup>-2</sup> with last contour shown only in the top panel.

night sky line emission, which was subtracted using an interactive routine in CIGALE. All regions for which PUMA velocities could be obtained are numbered in Figure 7 (*right*, SQ; *left*, NI). Velocities were obtained by PUMA for virtually all emission features seen in the Calar Alto IF images (Fig. 4), except for velocity-smearred emission in the shock. Table 2 lists PUMA-derived velocities for all SQ (col. [6]) and NI (col. [2]) emission regions that are numbered in Figure 7. Columns (3)–(4) list literature mea-

asures for comparison (CO and H I values can be found in the text). H $\alpha$  emission with SQ velocities in the range 6350–6414 km s<sup>-1</sup> is also detected in NI knots 18, 19, and 34. Column (3) lists velocities from Plana et al. 1999 whenever one of their possible velocities fell within  $\pm 100$  km s<sup>-1</sup> of our adopted value. Other literature values are given in column (4) (“h” denotes Gallagher et al. 2001; “f” denotes Arp 1973; “o” denotes corrected value for Ohyama, Nishiura, & Murayama 1998, which is contaminated by

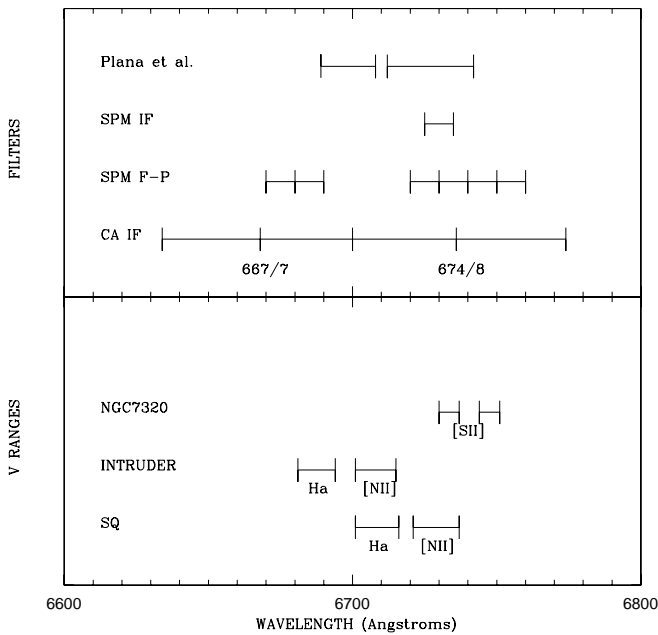


FIG. 6.—*Bottom*: Schematic shows the wavelength ranges for  $H\alpha$  and  $[N II] \lambda 6583$  emission in SQ and the new intruder as well as  $[S II] \lambda\lambda 6717, 6731$  emission in foreground NGC 7320. *Top*: Wavelength ranges sampled by various filters and Fabry-Pérot observations reported here and elsewhere. “Plana et al.” (*top*) refers to published CFHT and Russian 6 m Fabry-Pérot observations of Plana et al. (1999). SPM IF and CA IF refer to interference filter images obtained at San Pedro Martir and Calar Alto, respectively, while “SPM F-P” refers to Fabry-Pérot observations taken with PUMA at San Pedro Martir.

broad emission at SQ velocities; all others are from Moles, Marquez, & Sulentic 1998). Data quality is indicated by an asterisk, plus sign, or minus sign following a velocity, which correspond to  $1 \sigma$  uncertainties of 10, 20, and 30  $\text{km s}^{-1}$ , respectively. The latter usually correspond to regions where shock velocity smearing is seen. Fewer SQ velocities were

obtained because most emission in that velocity range is in/near the shock, where smearing and multiple velocity overlap often make reliable measurement uncertain or impossible.

All Fabry-Pérot velocities that overlap with  $H I$  emission clouds (see Fig. 5) show very close agreement with the  $H I$  derived velocities ( $H I$  velocities and channel maps are given in Williams et al. 2001). We note that a number of our velocities are in disagreement with those adopted by Plana et al. (1999). There are two reasons for this: (1) the much smaller free spectral range of the two Fabry-Pérot etalons that they employed led to three- or four-fold ambiguity about the correct source velocities, and (2) many/most of the emission regions south of NGC 7318ab have velocities outside of the range of their interference filters. Similarly, the apparent disagreement between our measures of two emission regions near or in common with Ohyama et al. (1998) result from their interpreting the strongest narrow-line component as  $H\alpha$ , when it is, in fact,  $[N II] \lambda 6583$ . The situation for the SQ velocity range is much more complex. All discrete source detections appear to correspond with  $H II$  regions imaged in Figure 4. Unlike the NI data, however, the SQ velocities and distribution of emission features show no concentration or hint of ordered motion. Emission features in the far northeast have been discussed in connection with the tidal tails produced by the OI. CO velocities for emission in (or projected on) NGC 7319 are given in § 4.1.4.

2.4. ISO Imaging

ISOCAM observations at 11.4 and 15  $\mu\text{m}$  were obtained on 1996 May 23 with the *Infrared Space Observatory (ISO)*. The 15  $\mu\text{m}$  observations were previously published in Xu, Sulentic, & Tuffs (1999), where details of the ISOCAM data reduction procedures can be found. We briefly summarize some key parameters that differ from the 15  $\mu\text{m}$  observations. The 11.4  $\mu\text{m}$  image was obtained using the

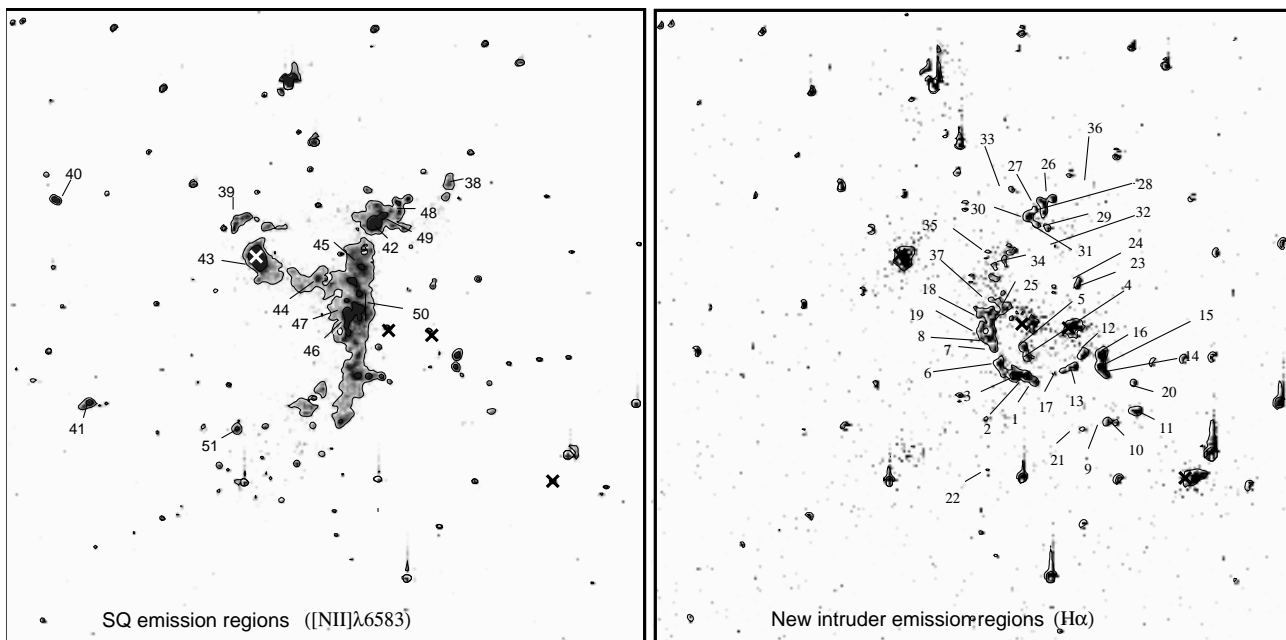


FIG. 7.—Identification charts ( $H\alpha$  contours) for all emission regions with measured velocities from our Fabry-Pérot observations for (*left*) SQ ( $[N II] \lambda 6583$ ) and (*right*) the NI ( $H\alpha$ ). Velocities for the identified features are found in Table 2.

TABLE 1  
NET COUNTS, FLUXES, AND LUMINOSITIES FOR THE DIFFERENT HRI COMPONENTS IN STEPHAN'S QUINTET<sup>a</sup>

COMP.	NET COUNTS			INTRINSIC X-RAY FLUX (ergs cm <sup>-2</sup> s <sup>-1</sup> )	X-RAY LUMINOSITY (ergs s <sup>-1</sup> )
	Old	New	Total		
Total $r < 3'$ .....	370 ± 48	833 ± 78	1203 ± 92	$6.1 \times 10^{-13}$	$5.3 \times 10^{41}$
Total $r < 1.5'$ .....	305 ± 28	703 ± 45	1008 ± 53	$5.1 \times 10^{-13}$	$4.5 \times 10^{41}$
Sey.....	45 ± 8	117 ± 13	162 ± 15	$8.2 \times 10^{-13}$	$7.2 \times 10^{40}$
Shock (int).....	66 ± 9	164 ± 15	230 ± 18	$1.2 \times 10^{-13}$	$1.0 \times 10^{41}$
Shock (ext).....	121 ± 15	338 ± 25	459 ± 29	$2.3 \times 10^{-13}$	$2.0 \times 10^{41}$
N7318a.....	24 ± 6	37 ± 8	61 ± 10	$3.1 \times 10^{-14}$	$3.7 \times 10^{40}$
NW ext.....	11 ± 5	28 ± 8	39 ± 9	$2.0 \times 10^{-14}$	$2.4 \times 10^{40}$
Residual $r < 1.5'$ .....	105 ± 22	183 ± 34	288 ± 41	$1.4 \times 10^{-13}$	$1.3 \times 10^{41}$

<sup>a</sup> Fluxes and luminosities in the 0.1–2.0 keV range are derived from the total count rates with a conversion factor of  $3.9 \times 10^{-11}$  ergs cm<sup>-2</sup> s<sup>-1</sup> and are corrected for the line-of-sight absorption. The usable integration time is  $t = 77.5$  ks.

ISOCAM long wavelength channel array ( $32 \times 32$  pixels) with the LW8 filter ( $\lambda_0 = 11.4 \mu\text{m}$ ,  $\delta\lambda = 1.3 \mu\text{m}$ ), which is sensitive to the unidentified broadband emission feature (UIB) at  $11.3 \mu\text{m}$ . Raster scans were made with  $\text{PFOV} = 6''$ ,  $M = 12$  steps,  $\delta M = 48''$  (in-scan) and  $N = 20$  steps,  $\delta N = 6''$  (cross-scan). The basic data reduction was done using the CAM Interactive Analysis (CIA) software.<sup>3</sup> The effective angular resolution of the image is  $10''$  (FWHM).

ISOPHT observations at  $60 \mu\text{m}$  were obtained using the C100 camera ( $3 \times 3$  pixels) on board *ISO*. The observations were carried out on 1996 May 23, using the ISOPHT oversampling mapping mode (P32) with an oversampling factor of 3. The map has 16 scan lines and nine pointings per map line, covering about  $13'$  (in scan)  $\times$   $6'$  (cross scan) on the sky. The  $60 \mu\text{m}$  map was reduced using the newest P32 data reduction package (Tuffs et al. 2001). This software takes advantage of the high sampling rate and high redundancy of P32 maps. The effect of detector transients were carefully

corrected. The angular resolution of the  $60 \mu\text{m}$  map is on the order of  $30''$ , which is  $\sim 50\%$  better than the detector pixel size ( $45''$ ). Figure 8a presents the  $11.4 \mu\text{m}$  image and Figure 8b the  $60 \mu\text{m}$  image with  $15 \mu\text{m}$  contours superposed. The group is resolved even at  $60 \mu\text{m}$ , where NGC 7319 and NGC 7320 are the strongest sources as with MIR wavelengths. Table 3 presents  $60 \mu\text{m}$  flux densities with estimated errors at least 30%. The total  $60 \mu\text{m}$  flux is 1.26 Jy, which is considerably higher than  $S = 0.89$  Jy obtained by *IRAS*.

### 2.5. VLA H II Mapping

SQ was mapped in the velocity range  $5511\text{--}6862 \text{ km s}^{-1}$  with the VLA in the C, CS, and D configurations and subsequent data reduction using AIPS. Details and complete sets of channel maps can be found in Williams et al. (2001). The integration ranges were  $5575.4\text{--}5810.5$ ,  $5917.5\text{--}6088.8$ , and  $6432.1\text{--}6776.1 \text{ km s}^{-1}$ . The resultant synthesized beam was  $23''.6 \times 17''.4$  with an rms noise in the maps of  $0.22 \text{ mJy}$  and a  $3 \sigma$  H I flux limit of  $0.015 \text{ Jy km s}^{-1}$ , corresponding to an H I column density of  $5 \times 10^{19} \text{ atoms cm}^{-2}$ . The H I mass detection limit is  $2.3 \times 10^7 M_\odot \text{ beam}^{-1}$  at the distance of SQ. H I contours for SQ ( $6500\text{--}7000 \text{ km s}^{-1}$ ) and

<sup>3</sup> CIA is a joint development by ESA Astrophysics Division and the ISOCAM Consortium led by the ISOCAM PI, C. Cesarsky, Direction des Sciences de la Matière, C.E.A., France.

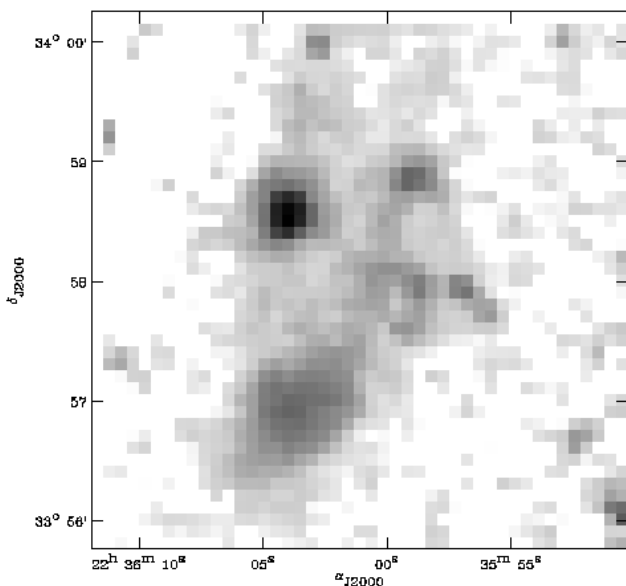


FIG. 8a

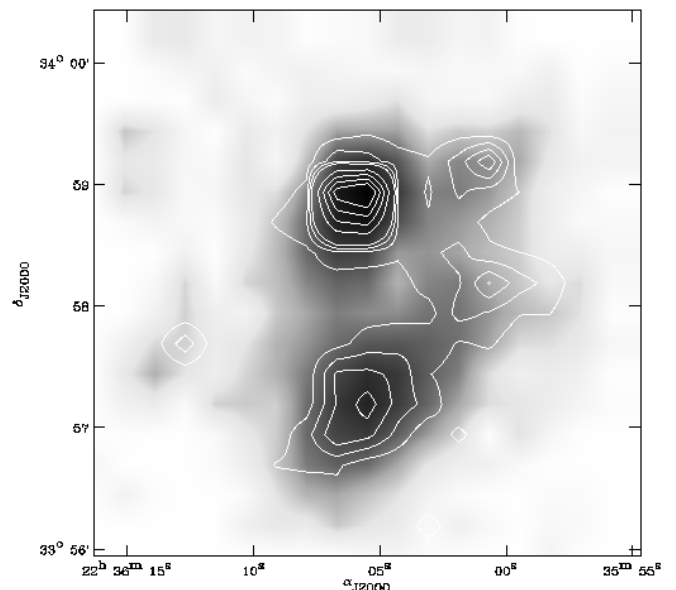


FIG. 8b

FIG. 8.—*ISO* images of SQ. (a)  $11.4 \mu\text{m}$  MIR ISOCAM and (b)  $60 \mu\text{m}$  FIR ISOPHT. Images are in log scale. The display range for the  $11.4 \mu\text{m}$  image is  $[0.01, 10] \text{ mJy pixel}^{-1}$  ( $6''$  square pixels). The  $15 \mu\text{m}$  contours are 0.1, 0.2, 0.3, 0.4, 0.8, 1.1, 1.4, and  $1.7 \text{ mJy}$  on a  $60 \mu\text{m}$  image with a display range  $[0.1, 10] \text{ mJy pixel}^{-1}$ . The bulk of the emission originates from the Seyfert 2 nucleus of NGC 7319 and the late-type foreground spiral NGC 7320.

TABLE 2  
FABRY-PÉROT (AND OTHER) VELOCITIES

INTRUDER				STEPHAN'S QUINTET		
Region No. (1)	F-P (km s <sup>-1</sup> ) (2)	Plana (km s <sup>-1</sup> ) (3)	Lit. (km s <sup>-1</sup> ) (4)	Region No. (5)	F-P (km s <sup>-1</sup> ) (6)	Identif./Notes (7)
1.....	5636*	...	5550h	38.....	7078+	
2.....	5635*	5580	5400h/5594f	39.....	6800*	
3.....	5680*	5640	5700h/5623f	40.....	6627+	
4.....	5640+	...	...	41.....	6617*	Starburst B
5.....	5708*	5715	5860e	42.....	6690*	Starburst A
6.....	5727*	5715	5717o/5540/6500h	43.....	6725*	NGC 7319 Seyfert nucleus
7.....	5766+	5740	6460	44.....	6422+	
8.....	5775*	5750	6460	45.....	6350/5987+	
9.....	5750*	...	...	46.....	6370-	
10.....	5737*	...	...	47.....	6370-	
11.....	5795*	5765	...	48.....	5990+	
12.....	5731*	...	...	49.....	6000+	
13.....	5699*	...	...	50.....	6350/6056+	
14.....	5766*	...	...	51.....	800+	NGC 7320 [S II]
15.....	5770*	5730				
16.....	5780*	5755				
17.....	5660*	...				
18.....	5810+	5815				
19.....	5830*	...				
20.....	5890*	5855				
21.....	5715+	...				
22.....	5860-	...				
23.....	5959*	...				
24.....	5921+	5935				
25.....	5940-	...				
26.....	5979*	5950	6020			
27.....	5990*	5960	6020			
28.....	5990*	...				
29.....	5988+	5960				
30.....	6017*	...				
31.....	6010*	5985				
32.....	6000-	...				
33.....	6017-	6005				
34.....	5987-	6000				
35.....	5997-	...				
36.....	6036-	...				
37.....	5959+	...				

the NI (5600–6000 km s<sup>-1</sup>) are overlaid on the corresponding H $\alpha$  interference filter images in Figure 5 (*top and bottom*, respectively).

A radio continuum image was also constructed by averaging all line-free channel maps. The effective radio continuum bandwidth was 2.05 Mhz with central frequency of 1416 Mhz. The rms noise was 0.10 mJy beam<sup>-1</sup>. The synthesized beamwidth is about 3 times larger than the highest-resolution continuum observations (van der Hulst & Rots 1981) but has about 3 times higher flux sensitivity. This map is shown in Figure 2*b*, where comparable resolution adaptively filtered X-ray contours are superposed.

#### 2.6. CFHT Imaging

Broadband *B* and *R* images were harvested from the 3.6 m Canada-France-Hawaii Telescope archive. The observations were obtained on 1993 August 21 with the MOS/SIS (multiobject spectrograph/subarcsecond imaging spectrograph) in direct imaging mode. Seeing was estimated

to be 0".8 (Plana et al. 1999). These archival data were kindly provided to us in reduced form by C. Mendes de Oliveira. The data were published by Mendes de Oliveira et al. (2001) with a different emphasis. The *B*- and *R*-band images represent the average of 5  $\times$  900 s and 6  $\times$  350 s exposures, respectively. The *B*-band image is shown in Figure 9*a*, while a *B*–*R* color map (see also Mendes de Oliveira et al. 2001) is shown in Figure 9*b*. CFHT provides the deepest images of SQ.

#### 2.7. HST WFPC Imaging

Broadband WFPC2 *B*, *V*, and *I* images for SQ were harvested from the *Hubble Space Telescope* archive and processed using the standard *HST* pipeline. Dithered sets of images were obtained on 1998 December 30 and 1999 June 17 with total exposure times for the *B* (F450W), *V* (F569W), and *I* (F814W) data sets of 6700, 3200, and 2000 s, respectively. One WFPC2 pixel equals 0".09 ( $\sim$  35–40 pc). The earlier pointing was centered on NGC 7318ab and NGC

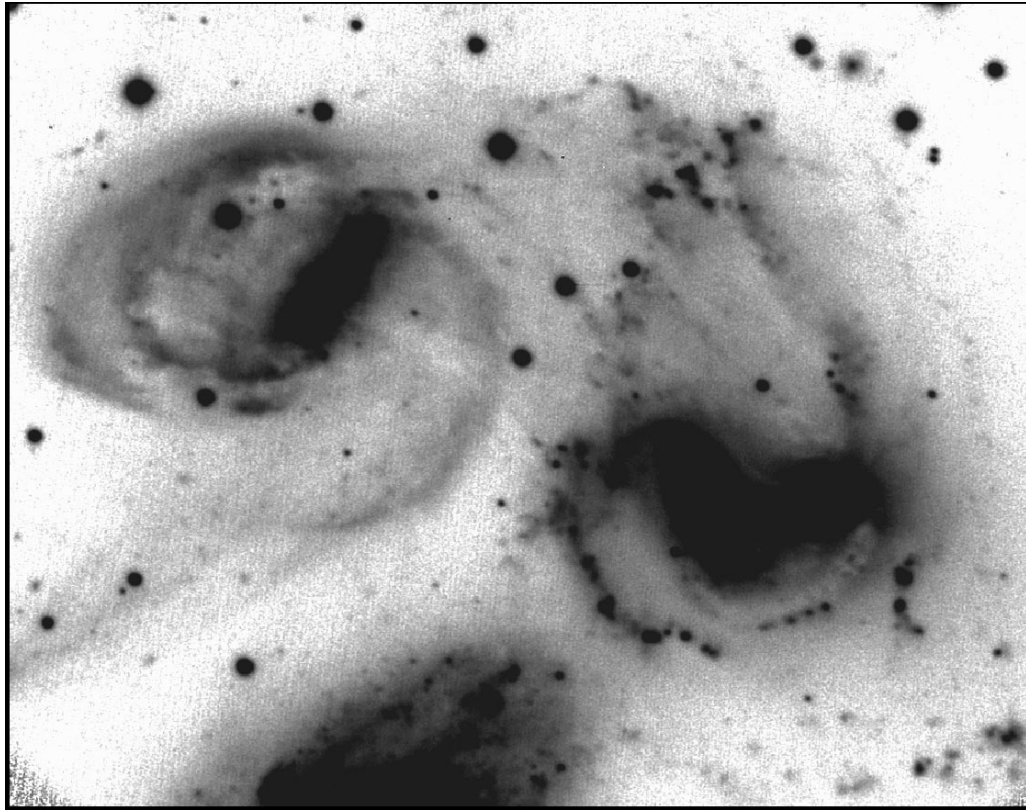


FIG. 9a

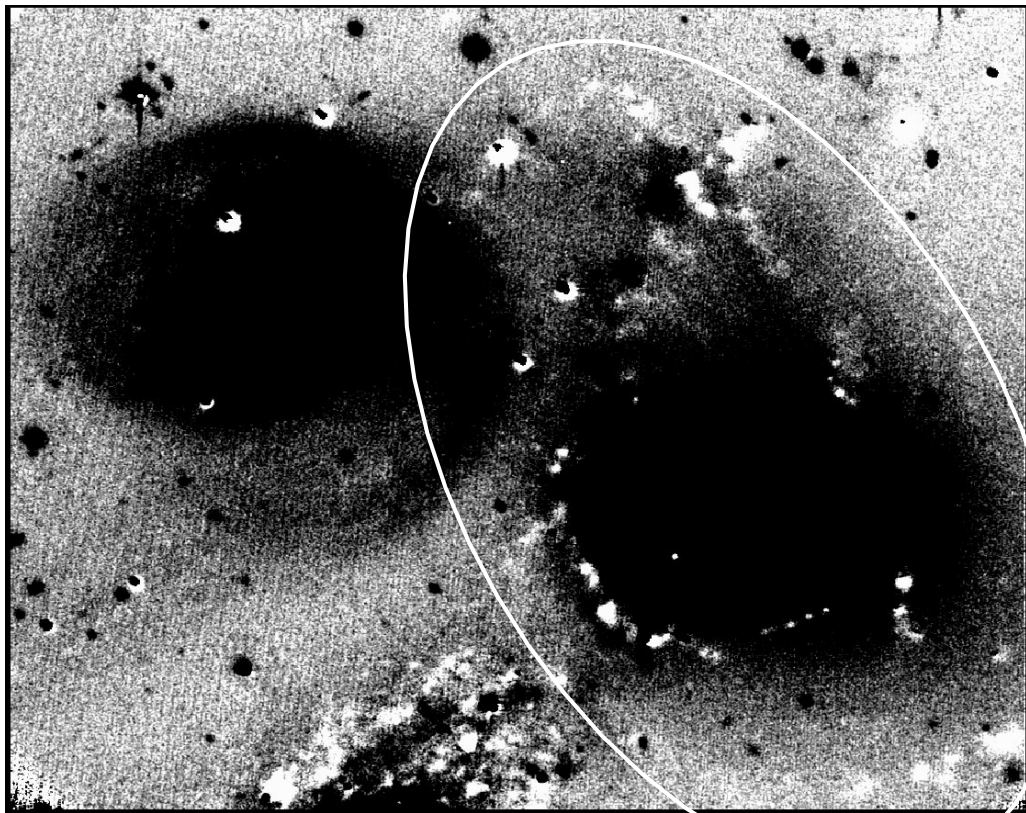


FIG. 9b

FIG. 9.—(a) CFHT  $B$  and (b)  $B-R$  images of SQ. The inferred size of the new intruder is indicated by an ellipse in (b) which is windowed to emphasize the bluest features (*white*). Using the same data, Mendes de Oliveira et al. 2001 measure  $B-R = 1.32$  for SQ starburst A and  $B-R = 0.4-0.7$  for the blue intruder emission regions north of it.

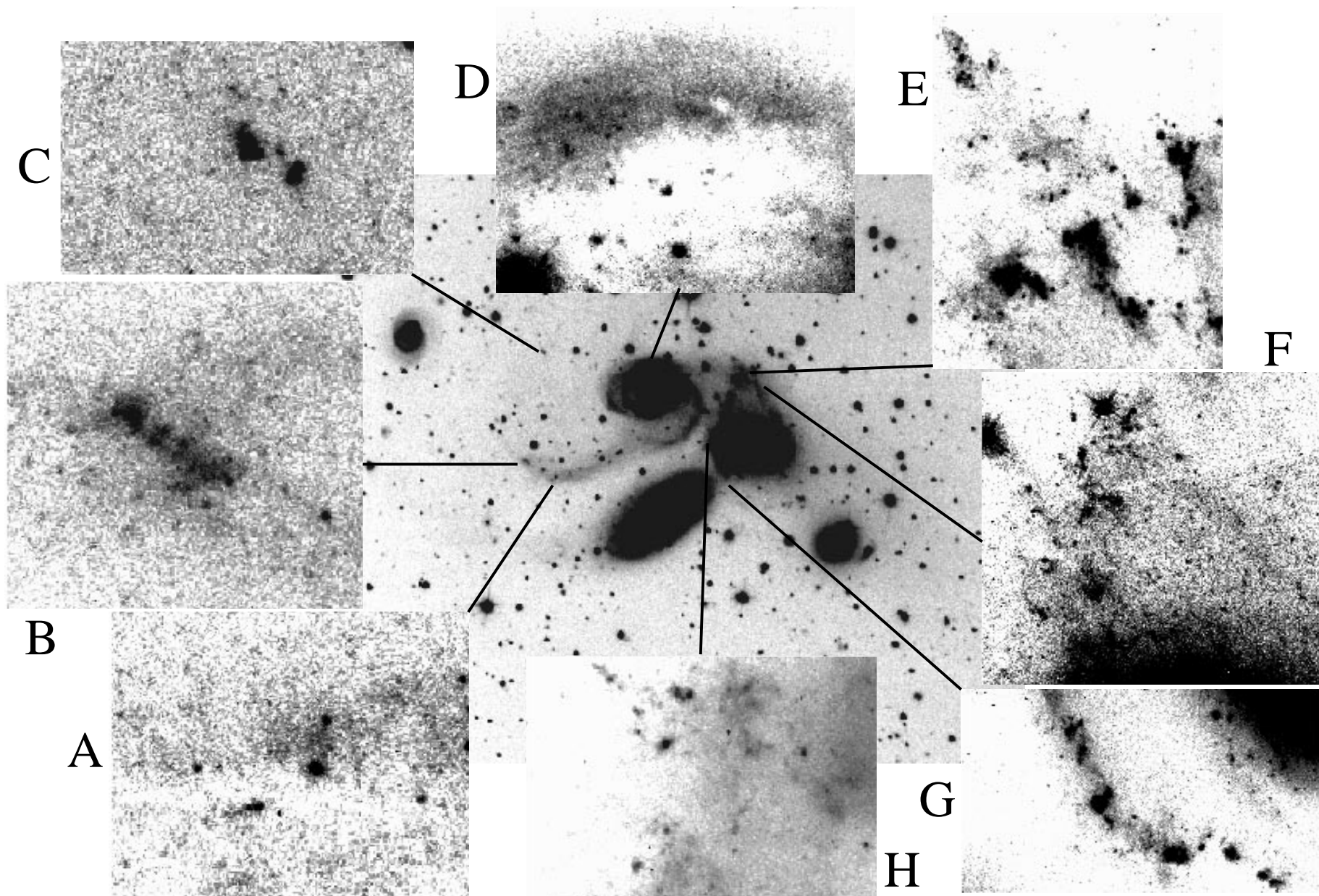


FIG. 10.—Vignettes of eight sources or regions in SQ taken from the average *B*-band WFPC2 image obtained with *Hubble Space Telescope*. The finding chart is an *R*-band image obtained with the CA 1.5 m telescope (see Moles et al. 1998). Vignettes show (a) the region of *ISO* starburst B in the younger tidal tail with associated dust lane; (b) very blue stellar concentration at the tip of the younger tidal tail. (c) Emission region near the north edge of the stripped H I cloud; (d) northeast corner of NGC 7319 showing a concentration of blue stars on the end of the ring as well as a large (possibly superposed) dust patch; (e) region of starburst A (*lower left*) and superposed intruder emission regions and dust lanes; (f) region of the new intruder and the shock front between starburst A and new intruder central bulge showing radial features (structural smearing or spokes as in the Cartwheel); (g) portion of the disrupted arm or ring of new intruder with ablating H II regions; (h) the center of the shock with debris of ablated H II regions and an emission ring (S edge).

TABLE 3  
ISO MIR AND FIR FLUXES

Source ID	$S_{11.4\mu\text{m}}$ (mJy)	$S_{60\mu\text{m}}$ (mJy)	$\log L_{60\mu\text{m}}$ $L_{\odot}$
NGC 7319 .....	47.5	529	9.83
NGC 7320 .....	59.8	487	7.92
NGC 7318ab.....	34.5	>24	>8.34
Starburst A .....	14.1	79.5	8.98
Starburst B.....	0.3	...	...

7319, while the later included NGC 7319 and the full extent of the younger tidal tail. Rather than show the entire field of view of the WFPC images, we have inset in Figure 10 high-resolution vignettes from the *B*-band image of the most interesting regions in SQ. The other utility of this data involves *B*–*V* colors for various components of SQ. These data were published by Gallagher et al. (2001) with a different emphasis. WFPC2 provides the highest-resolution images of SQ.

### 3. PREVIOUS MULTIWAVELENGTH RESULTS

#### 3.1. Radio

##### 3.1.1. Continuum Observations

Radio continuum observations of systems as distant as SQ should involve negligible thermal emission (e.g., foreground NGC 7320 is not detected) and should therefore be effective tracers of nonthermal processes, such as active galactic nuclei (AGNs) and shocks, both of which have often been attributed to galaxy-galaxy interactions. High-resolution observations (Kaftan-Kassim et al. 1975; van der Hulst & Rots 1981) resolved two continuum sources in SQ from an apparently unrelated source at the north edge of the group. SQ detections involve (1) the nucleus of the Seyfert 2 galaxy NGC 7319 and (2) an extended source in the region between NGC 7319 and the NI. The extended source has been interpreted as (1) the signature of an ongoing collision between NGC 7318a and NGC 7319, or (2) between NGC 7318a and NGC 7318b, as well as (3) a shock front involving a collision of the NI with something (Allen & Sullivan 1980; Shostak, Sullivan, & Allen 1984). In the former two scenarios the enhanced radio continuum feature would arise from a very large number of supernova remnants (van der Hulst & Rots 1981).

##### 3.1.2. Line Observations

H I measures are a sensitive diagnostic of the degree of dynamical perturbation in a galaxy or group of galaxies. High-resolution H I maps of SQ (Shostak et al. 1984; Verdes-Montenegro et al. 2000) reveal that almost all of the neutral hydrogen in SQ has been stripped from the component galaxies. Molecular gas content is strongly correlated with the star formation rate in a galaxy. High-resolution observations of SQ (Yun & Verdes-Montenegro 1997; Gao & Xu 2000; Smith & Struck 2001; Braine et al. 2001) indicate that CO emission is associated with (1) optically identified dust clouds (inside or superposed on NGC 7319) and (2) tidal debris produced by the intruders. While no measurable H I remains in NGC 7319,  $3\text{--}4 \times 10^9 M_{\odot}$  of  $\text{MH}_2$  are found along the same line of sight.

#### 3.2. Infrared

IR emission is a sensitive measure of star formation activity in a galaxy. This is especially true of MIR wavelengths where warm dust very close to star-forming regions is measured (Dultzin-Hacyan & Masegosa 1990). MIR radiation can be enhanced near sources of thermal (e.g., star formation) or nonthermal (e.g., AGN) photons. Deconvolved *IRAS* (Verdes-Montenegro et al. 1998; Allam et al. 1996) and ISOCAM observations (Xu et al. 1999 and Fig. 8, left) reveal that the bulk of the MIR emission in SQ arises from (1) the discordant redshift galaxy NGC 7320 (an Sd dwarf), (2) the nuclear region of NGC 7319, and (3) two detached and compact starbursts, one in a tidal tail produced by the OI and the other in the debris field associated with the NI (both involve strong CO detections, Smith & Struck 2001; Braine et al. 2001).

#### 3.3. Optical

##### 3.3.1. Broadband Imaging Observations

Broadband optical observations provide a direct measure of the interaction morphology of a pair or group through detection of tidal bridges/tails and diffuse light produced by dynamical stripping processes. Deep photographic images (Arp 1973) already revealed (1) the existence of two parallel tidal tails and (2) an envelope of diffuse starlight. The former features extend toward the OI and provide the best evidence that it has interacted with the group. The existence of two parallel tails suggests that it has been captured by SQ unless a single passage can produce both features. Surface photometry measures suggest that both tidal tails are quite blue (Schombert, Wallin, & Struck-Marcell 1990). An *R*-band measure of the luminous halo (Moles et al. 1998) suggests that  $L_{\text{halo}} = L^*$ , implying a tidal stripping timescale of about  $t \sim 1$  Gyr, assuming a reasonable rate of dynamical stripping (see e.g., Rabaca 1996). Two of the three core members of SQ (NGC 7317 and NGC 7318a) show elliptical morphology with colors *B*–*V*  $\sim 1.0$ , while NGC 7319 shows barred spiral structure but without significant evidence for an ISM (Zepf, Whitmore, & Levison 1991; Moles et al. 1998).

##### 3.3.2. Line Imaging, Photometry, and Spectroscopy

H $\alpha$  measures provide another direct measure of the star formation rate. Forbidden [N II]  $\lambda 6583$  emission is usually included in these measures and is more sensitive to shocks and nonthermal processes. Aside from the Seyfert nucleus, the other members of SQ show little or no nuclear H $\alpha$  emission (Vilchez & Iglesias-Paramo 1998a, 1998b; Iglesias-Paramo & Vilchez 1999, 2001; Severgnini et al. 1999). The strongest H $\alpha$  (and [N II]) emission feature in SQ lies between NGC 7319 and the NI, apparently associated with the radio synchrotron arc.

Very few published high-resolution and S/N spectroscopic observations exist for SQ. In part this is because the component galaxies lack significant emitting gas and absorption-line spectra for galaxies in the range  $B = 15\text{--}16$  requires long integrations and/or large apertures. This is especially true for the OI. An H I recession velocity in RC3 for this galaxy is spurious, while a single absorption-line spectrum reveals  $V = 6000 \pm 200 \text{ km s}^{-1}$ , implying a velocity difference of  $\sim 600 \text{ km s}^{-1}$  relative to SQ (see § 4.1 for a new value). Most published spectra involve H II regions near the radio continuum/H $\alpha$  arc or in the NI, which is the only SQ member to retain significant gas. New Palomar

5 m spectroscopy (Xu et al. 2001) along the north-south  $H\alpha + [N II]$  feature in SQ finds emission-line ratios consistent with shock excitation.

### 3.4. X-Ray

X-ray observations of compact groups provide another independent measure of high-energy phenomena, as well as information about a hot IGM component. SQ was originally thought to have a strong diffuse X-ray component (e.g., from thermally heated gas; Sulentic et al. 1995), but subsequent *ROSAT* HRI observations (Pietsch et al. 1997) revealed that most of the emission comes from the Seyfert nucleus and the region of the radio continuum and  $H\alpha$  arc. The X-ray observations support the interpretation of this feature as a shock interface between the SQ IGM and an NI infalling with a line-of-sight velocity  $v = 10^3 \text{ km s}^{-1}$ .

## 4. DISCUSSION

SQ is evolving through intergroup interactions, but especially through the effects of sequential intrusions by neighbors from the associated large-scale structure. The connection between ongoing and past events is very clear; the SQ ISM was produced/stripped in one or more of the past events involving the OI and part of it is now being shocked by a collision with the NI. The collision is unusual because of the large velocity difference between SQ and the NI ( $\Delta V \sim 10^3 \text{ km s}^{-1}$ ). Figures 2, 4, 5, and 8–10 show the new multiwavelength data supplemented with harvested archival observations. We amplify the evolutionary scenario advanced by Moles et al. (1997) by presenting old and new multiwavelength data that are largely consistent with it.

### 4.1. SQ Past History: Old Intruder

Past intrusions by the OI have significantly modified SQ and created the stripped gaseous environment that gives rise to the current shock and also contributed a significant mass of stripped stars to the common halo of the group (Moles et al. 1998).

SQ shows parallel tidal tails (Arp 1973; Arp & Lorre 1976), with 1' north-south separation ( $\sim 25 \text{ kpc}$ , assuming a distance of 90 Mpc), extending toward the OI. The existence of two tails suggests (1) that the OI has visited SQ at least twice and also (2) that it has been captured. The latter inference is confirmed by the low line-of-sight velocity difference between OI and SQ ( $\Delta V \sim 0 \text{ km s}^{-1}$ ) obtained from our F-P observations ( $V = 6583 \pm 20 \text{ km s}^{-1}$ ; confirmed by W. Keel 2001, private communication) showing that past estimates (implying  $\Delta V \sim 600 \text{ km s}^{-1}$ ) were too high. Hence the most recent encounter was slow, unless there is a very large transverse-velocity component.

#### 4.1.1. The Older Tail

We interpret the southern tidal tail as the older of the two because it is broader ( $\sim 9$  vs.  $5.5 \text{ kpc}$ ) and also shows lower optical surface brightness (our  $V$ -band estimate  $\mu = 26.0 \pm 0.5 \text{ mag arcsec}^{-2}$ ) versus  $\sim 24.4 \text{ mag arcsec}^{-2}$  (Schombert et al. 1990). The older tail appears to emanate from the southeast end of discordant redshift NGC 7320 (its full length is  $\sim 100 \text{ kpc}$  if it really extends from the southeast end of NGC 7320 to the OI, Arp 1973; Arp & Lorre 1976). This was one of the arguments used in the past for associating the discordant galaxy with SQ (Arp 1973). It probably passes behind NGC 7320 and connects to the

region of NGC 7318ab, unless it really is associated with NGC 7320. N7318b would not yet have arrived in SQ when this tail was formed. The new H I data support this hypothesis. H I contours shown in Figure 5 (*top*) indicate a gaseous counterpart to the old stellar tail that indeed passes behind NGC 7320 and terminates at the south edge of the shock zone. The eastern part of this H I tail skirts the south edge of the larger eastern H I cloud and appears to be morphologically and kinematically distinct from it with a continuous velocity gradient  $\sim 6560\text{--}6730 \text{ km s}^{-1}$  from east to west (south end of old stellar tail to south edge of the shock). The large eastern H I cloud shows less ordered velocities between  $6540\text{--}6670 \text{ km s}^{-1}$  (Williams et al. 2001).

The H I tail is connected via the shock zone with another (albeit denser and more compact) H I cloud to the north (Fig. 5, *top*) with similar velocity range ( $6700\text{--}6750 \text{ km s}^{-1}$ ). The connectivity in velocity is clear. The physical connectivity is also clear because the currently shocked gas was most likely H I before the arrival of the NI. We suggest that all of this material (north cloud, shock region, and H I tail behind NGC 7320) represents gas that was stripped in an earlier passage of the OI. The origin of this stripped gas might be ascribed to an encounter between the OI and one of the elliptical members (NGC 7317 or NGC 7318a). Certainly either of these galaxies could reasonably have been near the north end of this tidal structure  $\sim 1 \text{ Gyr}$  ago. The circumstantial evidence involves (1) an old stellar/H I tidal feature that most likely originated in an interaction between the OI and one or more SQ members and (2) an excess of early-type galaxies in SQ, which is found in a noncluster environment, where  $\geq 75\%$  late-type galaxies are expected. Indeed, most nearby members of the same large-scale structure component to which SQ belongs are spirals (see, e.g., Shostak et al. 1984). NGC 7319 is the only one of the three “core” SQ members (NGC 7317, NGC 7318a, and NGC 7319) that can be classified as a spiral. The continuity between the northern H I cloud, the shock zone, and the H I/old stellar tail behind the interloper motivates us to favor an origin for this structure in an earlier passage involving the OI. An interesting piece of evidence in favor of a two-intrusion hypothesis for production of the twin tails—via interaction with the OI—involves the observation that the older tail is not continuous (see Plate 6 in Arp & Lorre 1976). The fainter tail shows a clear bifurcation or “scalloping” ( $\sim 1.2$  from the south end of NGC 7320) just beyond the part that shows overlapping H I emission. This structure is qualitatively consistent with the hypothesis that the OI perturbed its older tail in the process of making the younger one.

One cannot rule out the possibility that the most recent passage of the OI split the H I disk of NGC 7319 ejecting gas both east and west. This possibility requires exploration with models. In this view at least some of the gas involved with the current shock originated in NGC 7319. We do not favor this view because it would leave the older tidal tail unexplained unless a single encounter can produce twin and parallel tails. It would also be difficult to account for the  $6700 \text{ km s}^{-1}$  H I cloud located northwest of NGC 7319. The continuity between this cloud, the shock zone, the H I tail behind the interloper NGC 7320, and the faint optical tail motivates us to favor an origin for this structure in an earlier passage involving the OI. This interpretation points toward an important significant role for secular evolution in compact groups.

#### 4.1.2. *The Younger Tail*

The younger (narrower and higher surface brightness) tail ( $\sim 40$  kpc in length) is primarily a stellar feature with H I overlapping only the outermost 10–15 kpc (Fig. 5, *top*). The H I does not conform to the shape of the stellar tail in the overlap region although the tail appears to curve along the inner side of the H I distribution where the H I intensity gradient is steepest. The younger tail connects directly with NGC 7319 leading us to assume that both the tail and H I cloud originated in the ISM of this galaxy and were stripped during the most recent encounter. The *B*-band CFHT image (Fig. 9a) shows that the tail is distinct from the southwest spiral arm, or broken ring, of NGC 7319 and suggests that the OI passed from northwest to southeast, parallel to and just west of the bar in NGC 7319. Figure 9a shows at least three distinct “streams” of stars extending from NGC 7319: one coming from the west arm, one from the direction of the central bar, and a central one (which most likely traces the path of the OI) from the interarm region. The streams converge into a single narrow tail about 10–20 kpc south-southeast of NGC 7319.

Star-gas decoupling in tidal tails has previously been attributed to interactions between the gaseous component and starburst winds (Heckmann et al. 1990) or with collisionally heated halo gas (Barnes & Hernquist 1996), neither of which is supported by our observations. The recent models show that such offsets arise naturally in low-inclination prograde encounters (Mihos 2001; see also Hibbard, Vacca, & Yun 2000). As observed, and expected from such models, the stellar and gaseous components are linked in the most distant parts. The decoupling sets in as material deeper in the galaxy is stripped with increasing effects of dissipation on the gaseous component (Mihos 2001). This suggests that the length of the pure stellar part of the tail should be a direct measure of the details of the encounter (relative velocity of intruder and orientation relative to the target disk). The data favor a low-velocity passage by the OI and at low inclination relative to the plane of NGC 7319 (see Gordon, Koribalski, & Jones 2001 for an opposite example). The data suggest that the earlier intrusion of the OI was of a different kind that did not lead to a star-gas decoupling.

The spiral structure in NGC 7319 is disturbed but not shattered. This observation and the fact that the stellar streams feeding into the tail appear to pass in front of the arm, suggest that the OI made a slow passage across (and above) the disk. The H I cloud coincident with the end of the younger tail is the most massive detected in SQ ( $M \approx 4.0 \times 10^9 M_{\odot}$ ). It shows velocities in the range 6540–6670  $\text{km s}^{-1}$  (see intensity contours in Fig. 5, *top*) consistent with an origin in NGC 7319. The cloud is better described as a “wall” of H I, rather than a tail, because it is uniformly displaced about one galaxy diameter east and south from NGC 7319. It extends more than 50 kpc north from the optical tail and the minimum separation between the west edge of the cloud and the east side of NGC 7319 is  $\sim 30$  kpc.

Little line-emitting gas remains inside NGC 7319, except for that associated with the AGN. Examination of Figure 4 (*top*) reveals a few weak H $\alpha$ -emitting regions associated with the stellar tail and H I cloud as follows: (1) two near the tip of the tail (see also Figs. 10a and 10b) and (2) a few small regions near the north end of the H I cloud (for the brightest see Fig. 10c). These emission regions are located just inside the SQ facing edge of the H I cloud where the intensity

gradient is steepest. One of the features in the tail (Fig. 10a) was detected by ISOCAM (Xu et al. 1999, source B). It is identified as star cluster candidate 7 in Gallagher et al. (2001). Our Fabry-Pérot measures yield a velocity  $V = 6617 \pm 20 \text{ km s}^{-1}$  for this region, consistent with the H I velocities in the area and with an origin in NGC 7319. This source shows MIR and H $\alpha$  fluxes about one-tenth as strong as in starburst A (Xu et al. 1999) that lies at the north edge of the shock. This implies a star formation rate of less than  $0.1 M_{\odot} \text{ yr}^{-1}$  for starburst B. This emission region may be heavily obscured as it is bisected by an opaque dust lane (see Figs. 4, *top*, and 10a). The emission regions in the tail are either remnants from a past star formation event associated with the creation of the tail or new condensations. WFPC2 images show that the weaker emission region (H $\alpha$  flux  $S_{\alpha} = 0.4 \times 10^{-15} \text{ ergs cm}^2 \text{ s}^{-1}$  or about 0.3 times starburst B) near the extreme tip of the tail (Fig. 10b) is involved with a bright segmented condensation of blue stars that extends for  $8'' = 3.6 \text{ kpc}$  along the tail. We measure  $B - V = 0.2$  (from the WFPC2 data) for this condensation.  $B - V$  colors in the paper were estimated relative to those reported for sources in Gallagher et al. (2001). Such a very blue  $B - V$  measure is found at the extreme end of the color sequence for peculiar and interacting galaxies (e.g., Larson & Tinsley 1978; Schombert et al. 1990) and is certainly consistent with the hypothesis that a very recent star formation event occurred there. Most of this star formation would have begun after the tail was formed (see age estimates below). The brighter H $\alpha$ -emitting region (starburst B)  $\sim 15$  kpc from the tip of the tail is much more gas/dust rich and is apparently in an earlier stage of starburst activity.

If these two regions are condensing in the tail then they are the best candidate for tidal dwarf formation in SQ. SQ has been frequently mentioned as a potential site for the formation of tidal dwarf galaxies (Hunsberger, Charlton, & Zaritsky 1996; Mendes de Oliveira et al. 2001; Iglesias-Paramo & Vilchez 2001; Gallagher et al. 2001; Braine et al. 2001). Models have successfully produced mass concentration in excess of  $10^8 M_{\odot}$  either inside, with subsequent ejection from interacting galaxies (Elmegreen et al. 1993) or tidally unbound debris (Gerola et al. 1983). Such a process takes time to develop (e.g.,  $10^8 \text{ yr}$  for significant star formation to occur; Elmegreen et al. 1993), which rules out all emission components west of the shock, where all time-scales are less than this value. We suggest that the local velocity gradients identified by Mendes de Oliveira et al. (2001) in or west of the shock are largely consistent with a larger scale velocity gradient (§ 4.2.2) that reflects the residual angular momentum in the NI disk. Some of the H II regions south of the NI are quite large ( $D \sim 400\text{--}500 \text{ pc}$ ), but, if our interpretation is correct, they are large because they are in the process of shock ablation. The best and probably only viable candidates in SQ involve starburst B and the blue concentration located, respectively, near or at the tip of the new tidal tail. Detection of significant CO emission (Braine et al. 2001) provides further support for the candidacy of starburst B near the end of the younger tail (Fig. 4, *top*, and Fig. 10a). All of the emission features on the east side of SQ fall on or near the inner side of the H I cloud where a relatively steep velocity gradient is observed (Fig. 5, *top*). The *HST* WFPC2 images suggest that all of the other candidate tidal dwarfs/emission regions in the tail are stars or background galaxies.

The most intriguing condensations are found near the

north end of the H I cloud that lies east of NGC 7319 (Fig. 5, *top*, and Fig. 10c). The two brightest objects are identified as star cluster candidates 30–31 (Gallagher et al. 2001), but their light is dominated by line emission (no line or continuum emission is detected in the H $\alpha$  IF image tuned to the NI velocity range). They are located more than 30 kpc east from that galaxy and north of the stellar tail. The very deepest photographic images (Arp 1973) reveal small condensations of luminous debris here as well as more filamentary structure. Such features are so faint that it is tempting to associate them with galactic cirrus (e.g., Sandage 1976). This is unlikely to be the case for the emission clumps detected in Figure 5 (*top*). Our Fabry-Pérot velocity measure for the brightest of these condensations ( $V = 6627$  km s $^{-1}$ ) agrees very well with H I velocities in the same area. This emission region shows a curious double structure (Fig. 10c) and is superposed on a faint linear feature (Plate 6, Arp & Lorre 1976) that extends toward the northeast. The most straightforward interpretation is that we are seeing the formation of extragalactic H II regions in the stripped ISM of NGC 7319.

#### 4.1.3. Estimating Ages for the Tails

An important chance to advance our understanding of the OI intrusions involves estimates of timescales. There are several ways to do this: (1) estimating the orbital period of the OI by using the tails as an orbital tracer, (2) estimating a diffusion timescale for the old tidal tail relative to the new one, and (3) using the colors of the blue tails to infer a timescale by assuming that the tails began with a starburst event. An even more simple-minded approach involves asking how long it would take material at the edge of the disk in NGC 7319 to reach the tip of the tail traveling at  $V \sim 200$  km s $^{-1}$  (assumed orbital velocity when inside NGC 7319) which yields  $t = 2 \times 10^8$  yr.

One can use the shape of the tails to extrapolate the projected orbit of the OI on the sky. The simplest approach for orbit estimation involves assuming an approximately circular orbit with projected diameter equal to the current distance between NGC 7319 and the OI ( $3' \sim 78$  kpc), which yields an estimated time  $t = 2.5 \times 10^8$  yr since the encounter with NGC 7319 and about  $7.5 \times 10^8$  yr since the old tail was produced. This estimate assumed  $\Delta V = 300$  km s $^{-1}$  between the OI and SQ. The bulk of this motion is assumed to be transverse since our Fabry-Pérot measure indicates that there is no significant line-of-sight velocity difference. The above timescale estimate represents a reasonable lower limit. The shape of the tails, and the clear evidence for a last perigalactic passage inside the west arm of NGC 7319, raise an interesting question about the baryonic center of mass in SQ. The obvious guess would be that the center of mass lies near the center of the light distribution, which would place it on or near to NGC 7318a and at least 20–40 kpc west of NGC 7319. The tidal tails then place it at least 1 galaxy diameter too far to the east. This may imply a very flat mass distribution and a center of mass ill defined or defined more by nonbaryonic than visible matter.

The old tail is fainter and more diffuse with a surface brightness similar to the feature found in the Centaurus cluster (Calcaneo-Roldan et al. 2000) but the conditions in SQ mimic a cluster environment in many ways. We assume here that one orbit ago the old tail was as broad as the young one. It is difficult to find quantitative estimates for the diffusion timescales of tidal tails. Recent models suggest

that tidal tails are more easily generated in shallow potentials (Dubinski et al. 1999). This is perhaps consistent with the previous discussion about the implied orbit of the OI. Surprisingly, in view of the nature of the encounters in SQ (and compact groups in general), close encounters are found to be more effective in generating straight tails (Dubinski et al. 1999). The models predict that most of the motion lies along the tail. The streaming seen in the young tail on CFHT and WFPC2 images certainly supports that expectation. Transverse motions in tails are generally expected to be quite small. If we assume a transverse velocity of 15 km s $^{-1}$  and ask how long it would take for the new tail to assume the width of the older one ( $\sim 4.5$  to  $\sim 9$  kpc), we obtain  $t = 2.5 \times 10^8$  yr.

It has been demonstrated that tidal tails are usually bluer than the galaxies involved in the interactions that produced them (similar to the colors of spiral galaxy disks from which most originate; Schombert et al. 1990). The bluest tails show  $B - V = 0.2$ – $0.4$ . We adopt 0.4 as a typical value for a young tail that still shows significant star formation. This assumption is supported by the  $B - V = 0.4$  measure (Schombert et al. 1990) for the source A starburst (Xu et al. 1999) involved with the ongoing collision in SQ. The same observations report  $B - V = 0.57$  for the younger tail consistent with a  $B - V = 0.2$  change in color. Estimates of the timescale for such a  $B - V = 0.2$  change (Wallin 1990; Bruzual & Charlot 1993; Calcaneo-Roldan et al. 2000) yield  $t = 2$ – $4 \times 10^8$  yr. This assumes that the star formation in the tail was quenched when the tails were formed. As discussed earlier, parts of the tail are much bluer presumably due to star formation initiated well after the tail was formed. This makes the inferred color change a lower limit to the age of the tail. We note that twisting is also predicted in some of the Wallin (1990) models. The WFPC2 images show clear evidence for twisting in the younger tail with a prominent twist being visible in the region shown in vignette A of Figure 10. A population of bright ( $M_V = -9$  to  $-11$ ) star cluster candidates have been identified (on the WFPC2 images) in the tail with ages ( $1 \times 10^7$  to  $5 \times 10^8$  yr), consistent with coeval formation with the tail or in succeeding star formation activity (Gallagher et al. 2001).

All estimates are consistent with an age for the new tail between 2 and  $4 \times 10^8$  yr, the event that stripped the ISM of NGC 7319. If we assume that this represents half an orbital period, then the old tail was produced 6–12  $\times 10^8$  yr ( $\approx 1$  Gyr) ago. SQ is particularly interesting because it contains both old and new tidal tails. This allows us to make cautious inferences about the probable evolution of a tail over a period of  $\sim 1$  Gyr. Other tails studied so far include those with estimated ages similar to both the old (Hughes et al. 1991; Mirabel, Lutz, & Maza 1991) and new (Mirabel, Dottori & Lutz 1992) SQ tails. The observed difference in surface brightness between the two SQ tails suggest that  $\leq 1$  Gyr will be sufficient for the older SQ tail to diffuse beyond detectability and, presumably, contribute to the diffuse stellar halo which in SQ is estimated to have an integrated luminosity  $\sim 1 L^*$  (Moles et al. 1998). SQ shows similarities with other tails as follows: (1) a dust component, (2) the site of significant star formation well after the tail was formed, and (3) blue condensations near the tip of the tail (Hughes et al. 1991; Mirabel et al. 1991, 1992). The dust feature in the SQ tail is much more well defined than the one seen in Leo triplet. WFPC2 images show it as a well-defined feature similar to the lanes observed in the disks of spiral galaxies.

The dust feature follows the edge of the presumably associated H I cloud and suggests that all components of the disk in NGC 7319 were pulled (unraveled) into the tail but shortly inside the innermost part of the dust lane the observed H I decoupling set in. The dust lane is either involved with or partially obscures starburst B, which is a reasonably strong MIR source (Fig. 8a). Perhaps the assumed older (Rots 1978) Leo triplet plume indicates that this younger dust feature will diffuse out over the next gigayear. The blue condensation at the tip of the SQ tail is the bluest of any studied in detail so far. The weakness of associated H $\alpha$  emission suggests that a burst of star formation recently ended here. The WFPC2 B-band image suggests possible decoupling of this feature from the rest of the tail while the V- and I-band images show much more continuity.

#### 4.1.4. NGC 7319 and 7320c: Spirals in Transition

The observations point toward a significant role for secular evolution of galaxy morphology in compact groups with spiral members likely being transformed into E/S0s. There is a clear analogy with the “galaxy harassment” process in clusters (e.g., Moore et al. 1996). The analogy is, of course even more appropriate for the NI with its cluster-like velocity relative to SQ. While we cannot prove that either NGC 7317 or NGC 7318a were originally spirals, NGC 7319 and NGC 7320c (and NGC 7318b) are clearly in morphological transition.

The fact that we can still classify NGC 7319 as a spiral (with a broken ring structure) galaxy is further support for our inferences that (1) it has not been involved in a direct collision and (2) it was stripped 0.2–0.6 Gyr ago. The latter inference is motivated by the fact that the spiral structure, while lacking emission regions, is still well defined, indicating that the last locus of star formation is still recognizable. The same can be said about the OI, which shows residual spiral structure and is classified RSXS0 in the RC3. Radial profiles of this galaxy reveal a bright central bulge surrounded by a disk/ring component. This structure is surrounded by low surface brightness emission with residual spiral arms. Both NGC 7319 and NGC 7320c have lost all/most of their ISM and the OI may also have lost its disk component. The H I disk of the OI is part of the old tidal feature discussed earlier. NGC 7319 has lost all detectable (upper limit  $\sim 10^8 M_\odot$ ) H I, the vast majority of H II regions (expected in a typical  $\sim$ SbB spiral) and an uncertain fraction of stellar mass. A few CO clouds have been detected across the face of NGC 7319 (Yun & Verdes-Montenegro 1997; Gao & Xu 2000; Smith & Struck 2001). They show little correspondence with the spiral arms and may simply involve debris above the plane of the disk and unrelated to the galaxy. Evidence supporting this suggestion involves the correspondence between the CO clouds and dust patches which can be seen in silhouette against the disk on deep images.

At this epoch NGC 7319 is without an ISM that could sustain the star formation necessary to propagate and define a Population I spiral pattern. The brightest condensation of young blue stars ( $B - V = 0.4 - 0.5$ ) are found on the northeast edge of the disk which is (1) just outside the largest H $\alpha$  + molecular gas concentration found along the line of sight to NGC 7319 and (2) on the side opposite from the inferred path of the OI. This condensation of H $\alpha$  and CO emission in NGC 7319 (Fig. 10d) is  $\sim 8$  kpc north-

northeast of the nucleus. CO and H $\alpha$  observations give consistent velocities,  $V = 6800 \pm 20$  km s $^{-1}$ , with an inferred H2 mass of  $4 - 7 \times 10^9 M_\odot$  (Yun & Verdes-Montenegro 1997; Gao & Xu 2000; Smith & Struck 2001). Star cluster candidates identified in this area (Gallagher et al. 2001) show colors consistent with ages in the range  $8 \times 10^6$  to  $1 \times 10^8$  yr.

The (V-band) luminosity of the younger tail  $L_{\text{tail}} = 0.10 - 0.15 L_{\text{N7319}}$ , which suggests that the most recent encounter contributed approximately that fraction of the total diffuse halo mass where  $L_{\text{halo}} \approx L^* \approx L_{\text{N7319}}$  (R-band measure, Moles et al. 1998). The B-band fraction would be considerably higher because (1) significant in situ star formation likely occurred after the tail was formed, and (2) the diffuse halo is considerably redder than the tail (Schombert et al. 1990; Moles et al. 1998). The OI is undetected in all H I surveys including the sensitive observations discussed here. In addition to morphological evidence that it is/was a spiral galaxy we can add the results of recent unpublished two-dimensional spectroscopic mapping at KPNO (W. Keel 2001, private communication) that reveals weak H $\alpha$  + [N II] emission showing ordered rotation. NGC 7319 and 7320c will presumably slowly transform into lenticular or elliptical (if interactions destroy the stellar disks) galaxies. This will enrich SQ with early-type galaxies. Such an excess of early-type E/S0 galaxies in compact groups is well established (Hickson et al. 1988), and there is little evidence that this excess might instead have arisen from mergers (Zepf et al. 1991). In about another gigayear SQ will have no spiral members unless another intruder arrives or NI loses a large amount of kinetic energy.

#### 4.1.5. The Seyfert 2 Nucleus of NGC 7319

The central region of NGC 7319 is luminous from X-ray to radio wavelengths. Most of this luminosity is assumed to be due to the type 2 AGN hosted there. A radio continuum survey of compact groups (including SQ) revealed a deficit of global radio emission from member galaxies, but an excess of compact nuclear emission in the spiral components (Menon 1995). While most of the gas will be stripped from galaxies in compact group environments, some undetermined quantity is efficiently channeled into component nuclei giving rise to active nuclei (Coziol, Iovino, & de Carvalho 2000). More recent high-resolution and high-S/N observations of the Seyfert 2 nucleus in NGC 7319 (Aoki et al. 1999) reveal a small-scale ( $\sim 5''$ ) triple-lobe radio continuum structure.

NGC 7319 contributes more than half of the MIR/FIR emission observed from SQ (Figs. 8a and 8b) which raises the following interesting questions: (1) should this flux be added to the FIR fraction assumed due to star formation? Or (2) does this emission arise from dust heated more or less directly by the nonthermal source? It is clear that the emission is thermal in origin because an extrapolation of the radio nonthermal power-law would not have been detected by IRAS or ISO (see radio continuum and IR fluxes in van der Hulst & Rots 1981; Allam et al. 1996; Verdes-Montenegro et al. 1998; Aoki et al. 1999). Without a star formation contribution from the nuclear region of NGC 7319, SQ shows a strong (FIR) deficit, rather than an excess in contrast to the interaction induced star formation enhancement that is observed, for example, in binary galaxies (Xu & Sulentic 1991). But this is not surprising given that almost all nonstellar matter in SQ is no longer bound

to individual galaxies. Conditions in the NGC 7319 ISM “debris field” north and east of the younger tail apparently do not favor condensation and star formation (at least in the first  $0.4 \pm 0.2$  Gyr)—except for a few isolated clouds inside and north of the younger tidal tail (§ 4.1).

Many Seyfert 2 nuclei show evidence for a near nuclear star formation enhancement. In fact some may not be AGNs at all (Dultzin-Hacyan & Benitez 1994). In the case of NGC 7319 there is little evidence for a nuclear starburst. *HST* images of the nuclear region (the central  $2'' \times 2''$ ; Malkan, Gorjian, & Tam 1998) show complex bright and dark spiral structure, but no evidence for star formation condensations. Radio continuum (Aoki et al. 1999) and supporting optical-slit spectroscopy (Aoki et al. 1996) shows evidence of complex internal jet plus triple-lobe structure on a scale of  $10''$ , but no signature of star formation. The high surface brightness structure seen in the inner kiloparsecs by WFPC2 is no doubt the source of the line emission seen on slit spectra. But this region is dominated by forbidden emission, rather than a starburst signature. We compared the stellar point-spread function (PSF) with the nuclear  $H\alpha + [N II]$  emission in NGC 7319. The PSF for stars in and near NGC 7319 on the average of our Calar Alto *R*-band continuum images (taken immediately after the emission line images) give a consistent FWHM =  $3''.5$  (the seeing was not good). The  $H\alpha + [N II]$  emission line PSF gives a similar PSF ( $3''.5$ – $4''.0$ ) except for a wing extending about  $10''$  to the southwest. The wing corresponds to the mostly forbidden emission studied by Aoki et al. 1996). The seeing disk therefore matches well the field imaged by WFPC2 where no evidence for significant starburst activity was found.

There is conflicting evidence for the presence of molecular gas in the nucleus of NGC 7319. Demonstration of significant molecular emission from the nucleus would support the argument that significant star formation was occurring there. Yun & Verdes-Montenegro (1999) detect a small cloud about 2 kpc south of the nucleus, but Gao & Xu (2000) place this source on the nucleus. We favor the former interpretation because the former (somewhat higher resolution) centering coincides with an optical dust patch seen in silhouette and the CO emitting region is clearly extended and not concentric with the nucleus. Thus it may well be a projected cloud of tidal debris rather than a concentration of molecular gas in the immediate nuclear region. In any case, the mass of molecular gas there is  $\leq 2 \times 10^8 M_\odot$ , inconsistent with the bulk of the observed MIR/FIR emission originating in a hidden nuclear burst. If one interprets the Seyfert 2 nucleus of NGC 7319 as a product of the most recent encounter with the OI then (1) only a small quantity of gas escaped the stripping event, (2) this small quantity was quickly and efficiently channeled into the innermost regions, (3) it gave rise to an AGN with associated small-scale radio lobes and an optical jet structure involving shocked gas, (4) little star formation is/was involved with this process, and (5) the dusty nuclear environment is likely heated more or less directly by the power-law continuum of the AGN, which reinforces our inference that the FIR signature of star formation in SQ is very weak.

#### 4.2. SQ: The Ongoing Collision

##### 4.2.1. The SQ ISM

We assume that NI was not inside or near SQ when the

interaction events described in the previous section transpired. Reasonable crossing times ( $t_c = 2$ – $8 \times 10^7$  yr) for NI are 5–10 times less than the estimated time since the last encounter between SQ and OI. Any shocks generated by past intrusions would have cooled, unless they involved very low density ( $n_e \sim 10^{-2}$ – $10^{-3}$  cm $^{-3}$ ) gas, and most interaction-induced star formation activity would have ended. We observe an X-ray and  $H\alpha + [N II]$  extension (Figs. 2c and 4, *top*) from the north-south-oriented shock zone toward NGC 7319. Its orthogonal orientation with respect to the shock motivates us to interpret it as related to the ongoing events. The most important inputs into our inferences about ongoing events involve (1) the configuration of the stripped ISM in SQ before the arrival of NI and (2) the trajectory and overall structure of NI. We suggest that Figure 5 (*top*) provides the most reasonable estimate of the immediate pre-shock SQ ISM. This superposition of H I (contours) on  $H\alpha + [N II]$  emission represents all warm and cold gas (except molecular) in the SQ velocity range.  $[N II]$  emission (Fig. 2d for the brightest part of the shock and Fig. 4 [*top*] for more extended diffuse emission) also traces the location of the hot gas. If one replaces the regions showing shocked gas with H I then one should have a reasonable idea of the preshock ISM.

Velocities of stars and gas associated with SQ span a range from 6400–7000 km s $^{-1}$  (Figs. 4 [*top*], 5 [*top*], and 7 [*left*]; Table 2). The gas surrounding NGC 7318ab spans the velocity range 5400–6000 km s $^{-1}$  (Figs. 4 [*bottom*], 5 [*bottom*], and 7 [*left*]). Therefore NI velocities are found in or west of the shock, while SQ velocities are found in, or east of, the shock. The only exception to this rule involves a radio, X-ray and  $H\alpha + [N II]$  extension (toward an emission condensation with an uncertain Fabry-Pérot  $V \sim 7000$  km s $^{-1}$ ) toward the extreme northwest of SQ. The SQ and NI emitting regions are reasonably well separated in the IF images shown in Figure 4.

We find H I clouds with unambiguously SQ velocities (Fig. 5, *top*): (1) north of the NI, (2) south of the NI, passing behind NGC 7320 and superposed on the old optical tail, as well as (3) the largest cloud located ESE of NGC 7319. Clouds 1 and 3 appear to be structurally and kinematically distinct, with cloud 2 part of an old tidal feature, perhaps involved with the stripping of NGC 7318a or NGC 7317, and cloud 3 involved with the more recently stripped ISM of NGC 7319. We suggest that clouds 1 and 2 are linked by the shock region where we find  $H\alpha + [N II]$  emission (Fig. 5, *top*). Gas in the region of the shock would have been largely cold (like H I clouds 1 and 2) before the arrival of the NI. This is a reasonable hypothesis because of the long estimated time since the last encounter and because of the small amount of  $H\alpha$  emission observed in optical and H I tidal features produced in past events (making it likely that little or no  $H\alpha$  in the shock region with SQ velocities is related to past events). One possible problem with this “linkage” involves the higher density and roughly circular shape of the northernmost H I cloud. We argue that the velocity continuity argument carries more weight. And the fact that at least a projected linkage is undeniable in the absence of the current shock conditions. Finally, the H I in tidal features is clumpy, and the north clump would be nearest the impact point that produced this assumed tidal feature.

The high-velocity passage of the NI through the stripped gas (the gas between components 1 and 2 above) gives rise to the shock. All relevant timescales connected with this

event are less than  $10^8$  yr (1) NI crossing time, (2) decay of the radio synchrotron emission ( $\sim 8 \times 10^7$  yr; van der Hulst & Rots 1981), (3) the shock cooling time, (4) the age of starburst A in SQ ISM on the north edge of the shock ( $1\text{--}2 \times 10^7$  yr, Xu et al. 1999), and (5) the ages of the bluest star cluster candidates identified in SQ (consistent with ages  $5\text{--}7 \times 10^6$  yr). Thus we assume that this is an ongoing collision. The implication of this assumption involves evidence in our data that (1) the ISM of the NI is not yet completely stripped, and (2) we are seeing NI H II regions in the process of ablation (see § 4.2.2).

The NI may have only grazed the H I feature, which is now partially shocked, given that its extreme line-of-sight velocity relative to SQ makes it unlikely that it has a very large transverse component. The fact that we detect both SQ and NI emission along the same line of sight at various places along the shock support this interpretation. If the elongated shock arose from a transverse, rather than line-of-sight, component in the NI velocity, we might expect to observe an eastward displacement of the SQ emission regions relative to those with NI velocities. Existing data find them along the same line-of-sight. In any case we cannot view the preexisting H I feature as a “wall,” but instead as an old tidal feature with well-defined extent. Of course we cannot rule out the existence of more extended H I (or X-ray emission) across a much wider part of SQ. In fact the large line-of-sight velocity difference makes it likely that the bulk of the shocked gas should be along the line of sight if there is any gas to shock in that direction. If present it may have a column density too low for detection (in H I or X-ray). The “missing” X-ray emission (see § 2.1) may originate in this line-of-sight component. Evidence for a more diffuse optical emission component comes from Figure 4 (*top*), where we see very extended and faint emission in addition to that associated with the north-south shock zone. It is reasonable to assume that most of this is probably diffuse [N II] emission.

Emission from the stripped ISM in SQ will involve two components as follows: (1) photoionization recombination emission (e.g., H $\alpha$ ) from denser emission regions associated with star formation and (2) forbidden emission from low-density shocked gas (e.g., [N II]  $\lambda 6583\text{\AA}$ ). Postshock emission regions can be distinguished from preshock NI emission by the considerable difference in velocity. Shocked gas will brake from near  $5600\text{--}6000$  km s $^{-1}$  to  $6400\text{--}6700$  km s $^{-1}$ . Optical emission from the shocked gas should follow the radio continuum and X-ray emission, and this is confirmed in Figure 2. Our Fabry-Pérot measures along the shock are often difficult to interpret. The forbidden [N II] emission is often so broad that it cannot be isolated as a line even with  $950$  km s $^{-1}$  free spectral range. Pre- and postshock emission regions are both detected in several places along the shock zone, where the Fabry-Pérot measures show two emission line peaks, one at NI ( $5400\text{--}6000$  km s $^{-1}$ ) and the other at SQ ( $6300\text{--}6400$  km s $^{-1}$ ) velocities. We may be detecting recoil in the shock zone because SQ velocities are  $\sim 300$  km s $^{-1}$  lower than unshocked H I north and south of the shock.

Comparison of ISO MIR 11.4 (Fig. 8*a*) and  $15 \mu\text{m}$  (Xu et al. 1999 and contours in Fig. 8*b*) with the H $\alpha$  images shows a weak correlation in the sense that only weak evidence for a MIR ridge or enhancement is seen along the shock zone. This is in marked contrast to the situation for galaxy pairs where FIR and especially MIR correlate strongly with

H $\alpha$  emission (Xu & Sulentic 1991; Hernandez-Toledo et al. 2001; Domingue 2001). MIR emission is weaker in the shock region than expected, for example from the shock/starburst A ratio for H $\alpha$  emission. The ratio of continuum subtracted H $\alpha$  flux (a  $100$  arcsec $^2$  region located  $40''$  south of starburst A for the shock measure) is  $R \sim 0.3\text{--}0.4 \pm 0.1$ , while the corresponding  $11.4 \mu\text{m}$  ratio is  $R \sim 0.14 \pm 0.1$ . Therefore we suggest that MIR emission may be suppressed in the shock region. If this is true then MIR/FIR measures will underestimate the star formation rate in the post shock gas. The weakness of the MIR emission along the shock may be telling us that much of the dust has been diffused and/or destroyed by sputtering in the shock region.

One very bright emission region is seen at the immediate edge of the north-south shock. ISOCAM starburst A with  $V = 6670$  km s $^{-1}$  is a strong source of H $\alpha$ + [N II], MIR (Xu et al. 1999), H I and CO (Smith & Struck 2001) emission. This is a complex region where both H I and CO spectra show two strong and narrow velocity peaks ( $6000$  and  $6700$  km s $^{-1}$ ). Our Fabry-Pérot measures indicate that all of the emission regions north of starburst A originate in the NI and account for the  $6000$  km s $^{-1}$  detections. Starburst A is either (1) a condensation of gas at the very edge of the most intense shock region (the SQ ISM at starburst A has been compressed but not shocked), or (2) it is an unusually dense region that has cooled out of the shock more quickly than adjacent regions. Local conditions have favored the conversion of much of the gas into molecules ( $M_{\text{H I}} = 1.5\text{--}5.0 \times 10^9 M_{\odot}$  and  $M_{\text{H}_2} = 1 \times 10^9 M_{\odot}$ ) (Smith & Struck 2001). It is difficult to give a reliable estimate for the H $\alpha$  intensity or equivalent width from our calibrated interference filter images. The relative strengths of starburst A and B (Xu et al. 1999) are more different than the EW values suggest (e.g., the starburst B/A EW ratio =  $0.74$  while the flux ratio =  $0.11$ ). The apparent EW similarity arises more because of the relative intensity of the adopted normalizing continuum. Both intensity and EW values also depend upon the correction for [N II] contamination which is maximally uncertain in the SQ shock region. Starburst A appears to be heavily reddened based on Figure 8*b*, where it is the only bright emission region that is distinctly red in color ( $B\text{--}R = 1.3$ , compared with  $B\text{--}R = 0.5\text{--}0.7$  in emission regions just north of it; Mendes de Oliveira et al. 2001). In fact this appears to be the effect of strong H $\alpha$ + [N II] emission in the R band because we derive  $B\text{--}V = 0.5 \pm 0.05$  from the WFPC data. In the absence of high-S/N slit spectra, the MIR data (Xu et al. 1999) are a more reliable estimator of the star formation rate in this case (B/A  $15 \mu\text{m}$  flux ratio =  $0.15$ , much more similar to the H $\alpha$  flux ratio). Starburst A at the edge of the shock region is almost 10 times more intense than starburst B at the end of a tidal tail produced  $\sim 4 \times 10^8$  yr ago.

#### 4.2.2. New Intruder ISM and Configuration

The main goal of this section is to discover the properties of the NI. It is difficult to construct a three-dimensional model of the galaxy because there is significant if not complete stellar-ISM decoupling. The stellar disk is traveling through SQ with such a high velocity that it probably remains little disrupted. Identifying the stripped disk of the NI is particularly difficult because (1) it will be projected on the bright galaxies and tidal debris in SQ, and (2) parts of the NI may pass around both sides of the H I clouds in its path and avoid being shocked at all. Our conclusion that

the NI ISM is not completely shocked is well supported by the Fabry-Pérot and H I data, which resolve considerable confusion about the nature of the nonstellar matter around NGC 7318ab. North and southwest of NGC 7318ab we see chaotic concentrations of emission regions in H $\alpha$  (Fig. 4, *bottom*), as well as the CFHT *B*-band image (Fig. 9a). They are even more clearly seen on the CFHT *B*–*R* image because of their blue color.

The bluest concentration of emission regions (we measure  $B - V = 0.3 - 0.5 \pm 0.05$  on the WFPC2 images) is seen just north and likely passing in front of starburst A (Fig. 10e). The equivalent emission regions to the south and southwest of NGC 7318ab are fainter (excluding the four largest and brightest condensations nearer to the center of the NI), which may indicate that they are on the far side of the NI and more affected by the complex dust lanes and patches that can be seen especially well on the CFHT and WFPC2 images. The optical feature extending northward from NGC 7318a toward the blue condensations (variously referred to as a tidal tail or arm) is confirmed as NI material by the detection of a few H II regions (at both ends) with velocities that are internally consistent and that connect smoothly to the northern emission regions. Figure 5 (*bottom*) shows the H I clouds with NI velocities as follows: (1) 5600–5800 km s<sup>-1</sup> located south-southwest of the nucleus and (2) 5960–6020 km s<sup>-1</sup> located north of the nucleus. Wherever H I clouds overlap (Fig. 5, *bottom*) we find excellent agreement between H I and Fabry-Pérot velocities. There is evidence for a residual rotation pattern in the NI emission regions over the range 5400–6000 km s<sup>-1</sup>: from 5400–5700 toward the south and southwest, increasing to 5800–6000 km s<sup>-1</sup> toward the west and north. Velocity gradients in the two H I clouds are consistent with this trend. The two distinct H $\alpha$  + H I concentrations suggest that the ISM of the NI has been split, in the sense that the gas between them has been shocked/displaced, but the angular momentum associated with this residual ISM has not been dissipated—further support for the hypothesis that the collision is ongoing. NI emission regions that collide with the SQ ISM at such high velocity will be shocked and ablated. At the same time H I will be rapidly heated in the shock. We therefore conclude that the complex H I + H $\alpha$  structure west of the shock involves H II regions either not yet shocked or ones that have missed the shock entirely. No emission around NGC 7318a (nothing west of the shock—except possibly at the extreme northwest edge of SQ) was found to have a velocity within 600 km s<sup>-1</sup> of the nuclear velocity of NGC 7318a. The lack of any emission regions attributable to NGC 7318a is consistent with its classification as an elliptical galaxy (see also Moles et al. 1998).

The deep CFHT images offer the best chance to make a reasonable estimate of the size and shape of the NI. On the *B* and *R* images we can detect much faint structure that is roughly symmetric about the central bulge of the NI. The northwest edge of the disk is particularly well seen with much faint flocculent structure. This structure trails in the same direction as the arm that extends from the edge of NGC 7318a toward the H II condensation north of starburst A. The southwest extent of the NI is indicated by the H I cloud and H $\alpha$  concentration (Fig. 5, *bottom*). The distribution of H II regions there is extremely chaotic. Pairs of very bright H II regions on the southwest side of the NI flank an apparent break in a ring or spiral arm. Emission

regions in the gap between the bright emission knots are displaced toward the southwest by several kiloparsecs. All of this region is enveloped by one of the NI H I clouds. Perhaps this region passed directly through NGC 7318a. The northernmost emission regions belonging to the NI extend north of starburst A and eastward from the shock near to the north edge of NGC 7319. Our *B*–*R* image (Fig. 9b) may provide the most valuable clue toward unraveling the outermost spiral arms in the NI. It shows a collection of faint blue condensations emerging from the southeast side of the central bulge/bar and passing across and south of the brightest H II regions mentioned above. This faint chain of emission regions passes across the north edge of NGC 7320. This feature connects with the H II concentration on the southwest edge. One region within NGC 7320 (region B1 of Arp 1973) and all regions to the southwest are confirmed to show NI velocities. We suggest that these emission regions trace the outermost NI spiral structure. In fact this feature connects more smoothly with the east end of the NI bulge/bar structure than does the bright string of emission regions closer to it. The latter appear to be most directly involved with the shock at this time.

The ellipse superposed on Figure 9b encloses all of the structure that belongs to the NI on the basis of kinematic or morphological continuity. The outermost southern spiral arm seen on the *B*–*R* image has a reasonably symmetric counterpart on the opposite side that involves the arm passing behind or in front of NGC 7318a and extending north of starburst A. CFHT and *HST* images suggest that this material is residual spiral structure—filamentary structure involving both bright and dark lanes are clearly visible here. All observations indicate that the NI is/was a large spiral galaxy especially given (1) the amount of atomic and molecular gas that can still be assigned to it and given (2) the residual rotation found in the velocity measures ( $\Delta V \sim 600$  km s<sup>-1</sup>). If we assume that the arms trail, the sense of rotation sees the north side nearest and receding. The major axis diameter of the ellipse in Figure 9b is  $\approx 2.6 \sim 65$  kpc and the minor axis  $\approx 1.6 \sim 40$  kpc, which implies an inclination to the line of sight in the range of 30°–40°.

The fact that (1) SQ shows an H I deficit despite the number of well defined H I clouds found there (Fig. 5; Williams et al. 2001) and (2) that almost one-third of our X-ray photons cannot be assigned to a discrete source provide some support for the hypothesis that there may be shocked gas across the broad extent of the NI (our upcoming Newton observations will be more sensitive to such emission). The well-defined arc that defines the shock in X-ray, radio continuum, and optical emission argues that part of the NI, the stripped part, may be east of the shock. Alternately, if the bulk of its motion is along the line of sight, one can argue that the edge of the NI is brushing past an old tidal H I feature as discussed earlier and suggested by Figure 5 (*top*). In this scenario a significant part of the NI may never be shocked. The strongest argument for a significant component of motion toward the northeast involves the extensive structural smearing seen in luminous and dust-related absorption features on the north and east side of the NI (Fig. 10f). One can see long luminous filaments extending for more than 20–30 kpc in Figure 9a. They extend from near the center of the NI toward the northeast. A prominent dust lane is the southernmost of these features, which extends from the NI directly toward the nucleus of

NGC 7319 (Fig. 9a; also visible on the photographs of Arp 1973). This structure does not look like residual spiral arms because it is too filamentary. The closest analogy one can find involves the spokes of the Cartwheel galaxy (Struck-Marcel & Higdon 1993; Struck et al. 1996). Perhaps the analogy to the Cartwheel is reasonable if the disk of the NI has passed directly through NGC 7318a.

We earlier proposed that the intrusion of the NI was not only recent but ongoing. Aside from the timescales cited earlier, the bright emission knots south of the NI and NGC 7318a may provide the most direct evidence. These features complicate any interpretation of the overall pattern of the NI. They appear anomalously bright and large (the largest show diameters of 400–500 pc) compared with other emission regions with NI velocities. One must concede to Arp (1973) that there are H II regions in SQ both larger and more luminous than any in NGC 7320 which is almost 10 times less distant. The southeast string of these emission regions appear to connect to the east end of the bar in the NI. Our CFHT *B–R* image suggests that instead a fainter arm passes from the bar and defines the south edge of the NI disk. The very bright features may perhaps be part of a disrupted internal ring. Whatever their origin we suggest that they represent NI emission regions in the process of ablation at the shock boundary. At this boundary H II regions will expand in directions perpendicular to the direction of motion, assuming a pancake-like shape as they become optically thin and dissipate. Little theoretical modeling exists for such a scenario, possibly because such a situation is likely to be rare. The more common but equivalent scenario involves emission knots in a hot stellar wind. In either case a large amount of NI kinetic energy will be converted into mechanical energy at the shock front. This energy will heat the SQ ISM as the NI emission regions are ablated, giving rise to the observed X-ray and forbidden optical emission. At the same time compression of the ISM and associated magnetic fields will increase the density of nonthermal electrons, giving rise to nonthermal radio emission. Some of the elongated emission features in the shock front resemble the expected shape of Rayleigh-Taylor instabilities or “fingers” that are expected in such a medium if the magnetic field lines are more or less perpendicular to the shock front and are compressing the gas against motion along the shock. A candidate instability feature is shown near the top of Figure 10h, but many can be seen on archival WFPC2 images.

If our interpretation is correct, then we have direct evidence for a shock component along the line of sight because the largest H II regions are west of the shock. If they are ablating then we know that the shock geometry is much more complicated than implied by the north-south “arc.” Surprisingly little high-S/N spectroscopy exists for emission regions in the NI. Two slit spectra, one published (Gallagher et al. 2001) and one unpublished (J. Gallagher 1999, private communication) exist for the region of the bright knots between the NI and foreground NGC 7320. These spectra show typical narrow emission-line-emitting H II regions with NI velocities. They also show very broad and diffuse emission regions with SQ velocities. Some evidence is also seen for more normal H II regions with SQ velocities. We interpret these as preshock, shock, and post-shock features. The published 10 m HET spectrum (Gallagher et al. 2001) intersects Table 2 emission regions 1, 2, and 3 and then passes just southeast of knot 6. The

former three regions show somewhat broad emission lines with unambiguously NI velocities. More diffuse gas between knots 3 and 6 shows velocity smeared emission (possibly at  $V \sim 6050 \text{ km s}^{-1}$ , intermediate between the NI and SQ) presumably at the shock front. The region just southeast of knot 6 (which has an NI velocity), shows weak somewhat diffuse emission at an SQ velocity. Our IF images (Fig. 4) show strong SQ and NI emission in this region. This is a part of the shock front where ongoing ablation is occurring. North of this region and inside the emission arc we see possible evidence of H II regions already destroyed in the form of diffuse disk- or ring-like features (see Fig. 10h and wider field archival WFPC2 images). The region where the H II region “ghosts” are seen lies directly east from the central regions of the NI where an X-ray, radio, and [N II] emission peak is observed. An alternative interpretation might view these features as supernova remnants. The SQ–NI interface appears to be an ideal laboratory for studying the ablation of emission regions in a shock.

## 5. SUMMARY AND IMPLICATIONS

### 5.1. *Galaxy by Galaxy*

Proceeding from west to east we summarize our interpretation of the evolutionary history for each galaxy in SQ. While some of these results were reported previously, most or all of our inferences benefit from the first-time unraveling of H I and H II velocities (from the Fabry-Pérot and H I measures) throughout SQ.

**NGC 7317:** an elliptical member linked to the rest of the group by diffuse stellar light (Moles et al. 1998). There is no evidence for its involvement in any of the events discussed above.

**NGC 7318a:** an early-type galaxy adjacent to the NI. The stars and gas in the old tidal tail may have originated in whole or part from this galaxy if it was transformed from spiral to elliptical type by an earlier encounter with OI. It is interesting that NGC 7318a is a stronger source at X-ray and radio continuum wavelengths, while NGC 7317 and NGC 7318b are not. Published *B*, *V*, and *R* magnitudes for these three galaxies (in the case of the NI we are referring to the luminous elliptical-like bulge component) differ by less than 0.5, while they show almost identical colors (Hickson, Kindl, & Auman 1989; Schombert et al. 1990; Moles et al. 1998). WFPC2 images show dust lanes crossing near the nucleus. This galaxy may be a good candidate for infall of tidal debris since the NI disk likely passed through it.

**NGC 7318b:** the NI is a large gas-rich spiral galaxy now entering SQ for the first time with line-of-sight velocity near  $1000 \text{ km s}^{-1}$ . It is entering the group from behind with a component of motion toward the east-northeast. Half or more of its ISM is now stripped. The residual ISM is split into two clouds of H I, H II regions and molecular gas with mean velocities near  $5700$  and  $6000 \text{ km s}^{-1}$ .

**NGC 7320:** a foreground Sd dwarf projected on the southern edge of SQ and directly upon the northern extension of the older tidal tail. H II regions associated with both SQ and the NI overlap its north end.

**NGC 7319:** an SBb spiral (with Sy2 nucleus) member that has lost most of its ISM. The new tidal tail appears to trace the passage of the OI from northwest to southeast. In the last intrusion the OI passed just west of the bar in NGC 7319 and above (or below) the disk. All detectable H I from NGC 7319 is now located in a complex cloud displaced

almost 1 galactic diameter east-southeast. One or two candidate tidal dwarf galaxies may be forming in this largely quiescent stellar and gaseous debris. Residual H $\alpha$  and (significant) H $_2$  gas are found in (or projected on) the northeast side of NGC 7319 opposite the path of the OI. Some of the gas that was not stripped may have fallen into the nucleus, thereby triggering the AGN. It is in transition from spiral to lenticular morphology.

**NGC 7320c:** the OI located one group diameter east-northeast shows evidence of a ring and spiral arms, but no trace of H I and weak optical line emission. It is interpreted as the OI because both optical tidal tails curve in its direction. It lost most of its ISM during a passage through SQ and is now bound to the group. It is in transition from spiral to lenticular morphology.

**SQ:** interactions in SQ are of two kinds: (1) nonimpulsive ( $\sigma_V \sim 0$ , line-of-sight, for NGC 7317, 7318a, 7319, and 7320c) quasi continuous interactions between bound members and (2) episodic highly impulsive intrusions by neighbors from the associated large-scale structure. It may be unusual that two intruders have visited SQ within the last gigayear, but the frequency will depend upon the richness of the associated large-scale structure and the mass of the attractor. In terms of galaxy surface density, SQ is not unusual (Sulentic 1987). Nonimpulsive interactions will create halos, possibly ignite AGNs, and dissipate angular momentum while the more violent collisions can modify member galaxies morphologically (ISM stripping, disk disruption, accelerating the halo-building process). Following this definition, both the OI and NI have been involved in interactions of the second kind. Either the OI lost a large amount of kinetic energy in the last visit or the close encounter with NGC 7319 was slow and remarkably efficient. The young tail and associated H I cloud supports the latter hypothesis. If the ISM of galaxies in SQ was largely lost to impulsive encounters then it will be dangerous to extrapolate the SQ experience to other groups, unless the dark matter (DM) haloes foster rapid and efficient dissipation of intruder kinetic energy.

SQ has survived significantly more than 1 Gyr without any evidence for onset of merging. As far as it goes this suggests that mergers may be very rare among compact groups. They must occur before the disruption/stripping process is too advanced or they will be unable to achieve extreme or even unusual IR luminosities (Borne, Bushouse, & Lucas 2000). SQ suggests that the proximity and strong interaction of four to five galaxies does not always lead to rapid coalescence although it does lead to efficient stripping of component ISMs. The latter results in depressed rather than enhanced star formation activity. It is unclear what role the episodic intrusions play in retarding the coalescence or whether the fate of the group is determined mostly by the properties of the DM halo thought to surround such groups. The observations suggest that it accounts for  $\sim 90\%$  of the mass (to accelerate high-velocity intruders) and that it is distributed very smoothly resulting in a very diffuse, rather than cuspy, potential.

## 5.2. Implications for High-Redshift Phenomena

Compact groups manifest the galaxy formation and evolution processes that are invoked to describe and explain what we see at high redshift. Interactions and the effects of interactions are believed to be more frequent in the past

(e.g., Wu & Keel 1998). Compact groups as the site of extreme interactions at low redshift may therefore be useful local analogs that can be studied in greater detail. We consider the implications of SQ to various topics often discussed in a high-redshift context.

1. Infall processes and structure formation in the universe: SQ suggests that compact groups form by the sequential acquisition of, sometimes high-velocity, intruders from the associated large-scale structure. Other Hickson groups also show internal high-velocity (likely) intruders and potential intruders just outside the isolation boundary (Sulentic 1987). We can identify with some confidence the two most recent (within the past 1 Gyr) arrivals in SQ. While not cataloged as a member of SQ, the OI is now likely bound to the system. The NI is likely a giant field spiral that we find in mid passage. The NI shows a cluster like velocity relative to SQ. If SQ is responsible for this high-infall velocity then a significant nonbaryonic mass component is required because the baryonic mass fraction in SQ is an order of magnitude too low to serve as an efficient attractor (Moles et al. 1997). Limits on the rapidity of formation and frequency of occurrence of this process will be set by the number of observed groups and the density of galaxies in their local environment.

2. Dynamical evolution: SQ shows classic signs of repeated interactions, such as tidal tails and diffuse light. SQ suggests that interaction with existing and incoming members leads to the gradual stripping of both gas and stars from group members. Two recognizable spirals in SQ are almost totally stripped: NGC 7319 and the OI are almost certainly evolving into E/S0 systems. SQ suggests that compact groups evolve from predominantly spiral to early-type systems. Early-type rich compact groups are found locally but their numbers, as evidenced by the Shakhbazian groups (e.g., del Olmo et al. 1995), appear to have been larger at higher redshift. The early-type rich compact groups would be the highly evolved analogs of SQ that are most resistant to merging. HCG79 (Seyfert's Sextet) may be the best low-redshift example. If such groups indeed originated from gas-rich spirals then the most intriguing question is, where did the gas go?

3. Star formation and ULIRGs: Compact groups do not show high average levels of star formation as inferred from their MIR/FIR emission (Sulentic & de Mello Rabaca 1993; Verdes-Montenegro et al. 1998). This is in contrast to what is seen in pair samples found in similar environments (e.g., Xu & Sulentic 1991). Dynamical evolution in SQ-like groups will leave most gas either too hot or too cold to support much star formation. In SQ the strongest residual starburst activity is of an unusual kind—modest starbursts in tidal debris. No Hickson group shows extreme IR properties (LIRG or ULIRG). Reasonably strong IR-emitting groups are often dominated by an AGN. In the case of SQ there is no evidence that even that IR emission is driven by star formation. The rare examples of high-redshift ULIRG compact groups (Borne et al. 2000) are likely different from the average Hickson (i.e., nearby) group. They are interpreted as multiple mergers in flagrante delicto while SQ shows no evidence for merger activity and much evidence for systematic metamorphosis from a spiral to an early-type rich system. Unless an ULIRG can form from a group that is largely stripped, they must be the most “unlucky” compact groups where component galaxies

arrive at about the same time (avoiding systematic disruption of the individual DM haloes) and quickly evolve to coalescence. Such groups are rare.

3. Feedback and the formation of AGNs: SQ contains a stripped spiral with Seyfert 2 nucleus that may have arisen because of the violent dynamical processes occurring there. The quasi continuous nature of the tidal torques in compact groups may more efficiently (than in pairs) channel gas into the nuclear regions of group members. This process, or feedback of stripped gas, could give rise to the excess of nuclear radio sources (Menon 1995) and type 2 AGNs (Coziol et al. 2000). It is perhaps too soon to expect more systematic feedback of stripped gas into the component galaxies of SQ. NGC 7318a may be the best candidate for tidal feedback since it is in the path of the NI disk. The general H I deficit found for the groups (e.g., Verdes-Montenegro et al. 2001) may be evidence that such feedback is very slow and inefficient.

4. Merger phenomena: A conservative age between 1–2 Gyr can be assigned to the identifiable episodes of intruder activity in SQ. SQ is dynamically evolved and all members except the ongoing intruder have lost their ISM. Unless significant gas feedback occurs, it is therefore difficult to envision a fate for SQ as an infrared bright (ULIRG) merger (Borne et al 2000). If one wants to make an ULIRG then one must do it quickly, before massive stripping occurs but after the dark matter halo is disrupted. If SQ is typical of compact groups then this requirement is rarely fulfilled. Yet the velocity dispersion in SQ  $\sigma_V \sim 0$  (excluding the unbound NI) is fairly common in local groups. Evolving

ideas about massive and diffuse DM halos around the groups may also be converging with observations that suggest that even low-velocity dispersion groups can resist merging indefinitely (Athanasoula, Makino, & Bosma 1997).

One of us (J. W. S.) acknowledges hospitality and support from IAA, OAB, and IdA, Universidad Nacional Autónoma de México (UNAM) during the course of this work, as well as support from NASA-JPL contract 961557. We acknowledge helpful discussions and assistance from I. Fuentes-Carrera, A. Iovino, A. del Olmo, and J. Perea. R. Tuffs is acknowledged for assistance with *ISO* data reduction. We thank C. Mendes de Oliveira for providing her CFHT images. The *HST* WFPC2 data were obtained from the multimission archive at the Space Telescope Science Institute (STScI). STScI is operated by the Association of Universities for Research in Astronomy (AURA), Inc., under NASA contract NAS 5-26555. L. V. M., is partially supported by DGI (Spain) grant AYA 2000-1564 and Junta de Andalucía (Spain). M. R. acknowledges grants 400354-5-2398PE of CONACYT and IN104696 of DGAPA-UNAM, Mexico. D. D.-H. acknowledges support from grant PAPIIT IN115599, UNAM. C. X. was supported by the Jet Propulsion Laboratory, California Institute of Technology, under contract with NASA. The *ROSAT* project is supported by the German Bundesministerium für Bildung, Wissenschaft, Forschung, und Technologie and by the Max-Planck-Gesellschaft.

## REFERENCES

- Allam, S., et al. 1996, *A&AS*, 117, 39  
 Allen, R., & Sullivan, W. 1980, *A&A*, 84, 181  
 Aoki, K., et al. 1996, *AJ*, 111, 140  
 ———, 1999, *ApJ*, 521, 565  
 Arp, H. 1973, *ApJ*, 183, 411  
 Arp, H., & Lorre, J. J. 1976, *ApJ*, 210, 58  
 Athanasoula, L., Makino, J., & Bosma, A. 1997, *MNRAS*, 286, 825  
 Barnes, J., & Hernquist, L. 1996, *ApJ*, 471, 115  
 Borne, K. D., Bushouse, H., & Lucas, R. 2000, *ApJ*, 529, L77  
 Braine, J., et al. 2001, *A&A*, 378, 51  
 Bruzual, A., & Charlot, S. 1993, *ApJ*, 405, 538  
 Calcaño-Roldán, C., et al. 2000, *MNRAS*, 314, 324  
 Coziol, R., Iovino, A., & de Carvalho, R. 2000, *AJ*, 120, 47  
 del Olmo, A., et al. 1995, in *ASP Conf. Ser. 70, Groups of Galaxies*, ed. O.-G. Richter & K. Borne (San Francisco: ASP), 117  
 Domingue, D. 2001, Ph.D thesis, Univ. Alabama  
 Dubinski, J., et al. 1999, *ApJ*, 526, 607  
 Dultzin-Hacyan, D., & Benitez, E. 1994, *A&A*, 291, 720  
 Dultzin-Hacyan, D., & Masegosa, G. 1990, *A&A*, 238, 28  
 Elmegreen, B. G., Kaufman, M., & Thomasson, M. 1993, *ApJ*, 412, 90  
 Gallagher, S., et al. 2001, *AJ*, 122, 163  
 Gao, Y., & Xu, C. 2000, *ApJ*, 542, L83  
 Gerola, H., Carnevali, P., & Salpeter, E. 1983, *ApJ*, 268, 75  
 Gordon, S., Koribalski, B., & Jones, K. 2001, *MNRAS*, 326, 578  
 Heckmann, T., Armus, L., & Miley, G. 1990, *ApJS*, 74, 833  
 Hernandez-Toledo, H. M., Dultzin-Hacyan, D., & Sulentic, J. 2001, *AJ*, 121, 1319  
 Hibbard, J., Vacca, W., & Yun, M. 2000, *AJ*, 119, 1130  
 Hickson, P. 1982, *ApJ*, 255, 382  
 Hickson, P., et al. 1988, *ApJ*, 331, 64  
 Hickson, P., Kindl, E., & Auman, J. 1989, *ApJS*, 70, 687  
 Hughes, D., et al. 1991, *Ap&SS*, 177, 199  
 Hunsberger, S., Charlton, J., & Zaritsky, D. 1996, *ApJ*, 462, 50  
 Iglesias-Paramo, J., & Vilchez, J. M. 1999, *ApJ*, 518, 94  
 ———, 2001, *ApJ*, 550, 204  
 Iovino, A. 2000, in *IAU Colloq. 174 Small Galaxy Groups*, ed. M. Valtonen & C. Flynn (ASP Conf. Ser. 209) (San Francisco: ASP), 25  
 Kaftan-Kassim, M., Sulentic, J., & Sista, G. 1975, *Nature*, 253, 176  
 Larson, R., & Tinsley, B. 1978, *ApJ*, 219, 46  
 Le Coarer, E., et al. 1993, *A&A*, 280, 365  
 Malkan, M., Gorjian, V., & Tam, R. 1998, *ApJS*, 117, 25  
 Mendes de Oliveira, C., et al. 2001, *AJ*, 121, 2524  
 Menon, T. K. 1995, *MNRAS*, 274, 845  
 Mihos, C. J. 2001, *ApJ*, 550, 94  
 Mirabel, F., Dottori, H., & Lutz, D. 1992, *A&A*, 256, 19  
 Mirabel, F., Lutz, D., & Maza, J. 1991, *A&A*, 243, 367  
 Moles, M., Marquez, I., & Sulentic, J. W. 1998, *A&A*, 334, 473  
 Moles, M., Sulentic, J. W., & Marquez, I. 1997, *ApJ*, 485, L69  
 Moore, B., et al. 1996, *Nature*, 379, 613  
 Ohyama, Y., Nishiura, S., & Murayama, T. 1998, *ApJ*, 492, L25  
 Pfeffermann, E., et al. 1987, *SPIE*, 733, 519  
 Pietsch, W., Trinchieri, G., Arp, H., & Sulentic, J. W. 1997, *A&A*, 322, 89  
 Pietsch, W., Trinchieri, G., & Vogler, A. 1998, *A&A*, 340, 351  
 Plana, H., et al. 1999, *ApJ*, 516, L69  
 Prandoni, I., Iovino, A., & MacGillivray, H. T. 1994, *AJ*, 107, 1235  
 Rabaca, C. R. 1996, Ph.D. thesis, Univ. Alabama  
 Rood, H., & Williams, B. 1989, *ApJ*, 339, 772  
 Rosado, M., et al. 1995, *Rev. Mex. Astron. Astrofis. Ser. Conf.*, 3, 268  
 Rots, A. H. 1978, *AJ*, 83, 219  
 Sandage, A. 1976, *AJ*, 81, 954  
 Schombert, J., Wallin, J., & Struck-Marcell, C. 1990, *AJ*, 99, 497  
 Severgnini, P., et al. 1999, *A&AS*, 137, 495  
 Shostak, G. S., Sullivan, W. T., III, & Allen, R. J. 1984, *A&A*, 139, 15  
 Severgnini, P., et al. 1999, *A&AS*, 137, 495  
 Smith, B., & Struck, C. 2001, *AJ*, 121, 710  
 Struck-Marcell, C., & Higdon, J. 1993, *ApJ*, 411, 108  
 Struck, C., et al. 1996, *AJ*, 112, 1868  
 Sulentic, J. W. 1987, *ApJ*, 322, 605  
 Sulentic, J. W. 1997, *ApJ*, 482, 640  
 ———, 2000, in *IAU Colloq. 174 Small Galaxy Groups*, ed. M. Valtonen & C. Flynn (ASP Conf. Ser. 209) (San Francisco: ASP), 226  
 Sulentic, J. W., & de Mello Rabaca, D. 1993, *ApJ*, 410, 520  
 Sulentic, J. W., Peitsch, W., & Arp, H. 1996, 5, *A&A*, 298, 420  
 Trinchieri, G., et al. 2001, in preparation  
 Trümper, J. 1982, *Adv. Space Res.*, 2 (4), 241  
 Tuffs, R., et al. 2001, preprint  
 van der Hulst, J. M., & Rots, A. H. 1981, *AJ*, 86, 1775  
 Verdes Montenegro, L., et al. 1998, *ApJ*, 497, 89  
 ———, 2000, in *IAU Colloq. 174 Small Galaxy Groups*, ed. M. Valtonen & C. Flynn (ASP Conf. Ser. 209) (San Francisco: ASP), 226  
 ———, 2001, *A&A*, 377, 812  
 Vilchez, J. M., & Iglesias-Paramo, J. 1998a, *ApJ*, 506, L101  
 ———, 1998b, *ApJ*, 508, 248  
 Voges, W., et al. 1992, in *European International Space Year Conference*, ed. T. Guyonne & J. Hunt (Saint-Mandé: Soc. française), 223  
 Wallin, J. 1990, *AJ*, 100, 1477  
 Williams, B., et al. 2001, *ApJ*, submitted

Wolter, A., Trinchieri, G., & Iovino, A. 1999, *A&A*, 342, 41  
Wu, W., & Keel, W. 1998, *AJ*, 116, 1513  
Xu, C., & Sulentic, J. W. 1991, *ApJ*, 374, 407  
Xu, C., Sulentic, J. W., & Tuffs, R. 1999, *ApJ*, 512, 178

Xu, C., et al. 2001, in *ASP Conf. Ser. 240, Gas and Galaxy Evolution*, ed.  
J. Hibbard, M. Rupen, & J. van Gorkom (San Francisco: ASP), 594  
Yun, M. S., & Verdes-Montenegro, L. 1997, *ApJ*, 475, L21  
Zepf, S., Whitmore, B., & Levison, H. 1991, *ApJ*, 383, 542